DISSERTATION

Macrophage and Monocyte Responses to SARS-CoV-2

Analyse SARS-CoV-2-induzierter Makrophagen- und Monozytenphänotypen

zur Erlangung des akademischen Grades
Medical Doctor - Doctor of Philosophy (MD/PhD)

vorgelegt der Medizinischen Fakultät
Charité – Universitätsmedizin Berlin

von

Daniel Christian Wendisch

Erstbetreuung: Prof. Dr. med. Leif Erik Sander

Datum der Promotion: 29.11.2024

Inhaltsverzeichnis

Tabellenverzeichnis

Abbildungsverzeichnis

Abkürzungsverzeichnis

ARDS	Acute respiratory distress syndrome
BAL	Bronchoalveolar lavage
CT	Computed tomography
CyTOF	Cytometry by time of flight
DAD	Diffuse alveolar damage
DGE	Differential gene expression
ECMO	Extracorporeal membrane oxygenation
EM	Transmission electron microscopy
FCS	Furin cleavage site
FDR	False discovery rates
FOV	Field of view
H&E	Hematoxylin-eosin
ICU	Intensive care unit
IL-6	Interleukin 6
LGMN	Legumain/Asparagine endopeptidase
MCFC	Multi-color flow cytometry
MELC	Multi-epitope ligand cartography
MHC II	Major histocompatibility complex type II
MOI	Multiplicity of infection
MPS	Mononuclear phagocyte system
MS	Mass-spectrometry
Mφ	Macrophage
NRP1	Neuropilin 1
PBMC	Peripheral blood mononuclear cells
PC	Principle component
PCA	Principal component analysis

PCR	Polymerase chain reaction
PDGF	Platelet-derived growth factor
scRNA-seq	Single cell RNA sequencing
scVI	Single cell variational inference
sn-RNAseq	Single-nucleus RNA-sequencing
TGF-β	Transforming growth factor beta
UMI	Unique molecular identifiers
Vcin	Inspiratory vital capacity
vvECMO	Veno-venous extracorporeal membrane oxygenation

Zusammenfassung

Seit Beginn der COVID-19-Pandemie stellt sich die Frage, inwiefern sekundäre Immunprozesse den Lungenfunktionsverlust bei COVID-19 aggravieren. Makrophagen und deren potenzielle Vorläufer, die Monozyten, sind wichtiger Bestandteil der antiviralen Immunabwehr und Wächter der Gewebshomöostase. In den Arbeiten, die dieser Promotion zugrunde liegen, wurden daher Assoziationen von Makrophagen- und Monozyten-Phänotypen mit der Krankheitsschwere von COVID-19 analysiert. Beide Studien umfassten jeweils eine Hypothesen-generierende Phase gefolgt von einer Validierungsphase in jeweils zwei separaten Kohorten und erfolgten im ersten Jahr der Pandemie in Deutschland.

In Publikation B dieser Dissertation wurden humane Leukozyten in insgesamt 242 Blutproben von 109 Spendern mit COVID-19 untersucht. Mithilfe multiparametrischer Methoden, wie der Einzelzell-RNA-Sequenzierung (scRNA-seq) und Zytometrie-mittels-Flugzeitmessung (CyTOF), konnten deutliche Unterschiede in den Monozyten-Phänotypen zwischen schweren und milden Krankheitsausprägungen detektiert werden. Milde COVID-19-Erkrankungen waren durch $CD14^{+}$/HLA-$DR^{hi/}CD83^{hi}$-Monozyten gekennzeichnet, die Monozyten einer Vergleichsgruppe mit grippalen Infekten ähnelten. Im Gegensatz hierzu besaßen Monozyten bei schweren Verläufen prädominierend einen $CD14^{+}$/HLA-DR^{lo}/$Calgranulin^{hi}$-Phänotyp mit verminderter Expression antiviraler und inflammatorischer Gene. Monozyten von COVID-19-Patienten exprimierten mehr CD163.

In Publikation A wurde die Genexpression pulmonaler Makrophagen von 47 Spendern mit akutem COVID-19 Atemnotsyndrom (ARDS) mithilfe von scRNA-seq, massenspektrometrischer Proteomik sowie multiparametrischer Mikroskopie untersucht. Die Anzahl CD163-positiver Makrophagen war im Lungengewebe verstorbener COVID-19-Patienten signifikant erhöht. Ebenfalls war in frühen Krankheitsstadien ein CD163/LGMN-positiver Phänotyp der Makrophagen (Mφ) in broncho-alveolären Lavagen prädominant. Auffällig war, dass CD163/LGMN-Mφ weniger durch Expression von antiviralen oder inflammatorischen Genen gekennzeichnet waren, jedoch durch Expression von Fibrose-assoziierten Gensignaturen. Ausgeprägte Ähnlichkeiten zwischen publizierten Makrophagen-Phänotypen bei pulmonaler Fibrose im Vergleich zu CD163/LGMN-Mφ, waren wesentlich auf

die Genexpression von LGMN und SPP1 zurückzuführen und - trotz hoher Expression - weniger auf CD163.

Bemerkenswerterweise wurden diese Fibrose-assoziierten Signaturen gleichermaßen in vitro in primären humanen Monozyten durch SARS-CoV-2 (D614G Indexstamm) induziert. Dieser Phänotyp unterschied sich deutlich von jenem nach Stimulation mit Influenza A Viren beziehungsweise nach Stimulation inflammatorischer beziehungsweise antiviraler Immunrezeptoren.

Zusammenfassend waren Makrophagen- und Monozyten-Phänotypen bei schwerem COVID-19 früher Varianten nicht durch Expression prototypischer antiviraler Gene gekennzeichnet, jedoch durch Expression von Calgranulin beziehungsweise Fibrose-assoziierten Genmodulen.

Abstract

Macrophages and monocytes are integral in the initiation and resolution of antiviral processes and controllers of tissue homeostasis. While SARS-CoV-2 can impede pulmonary tissue function merely by infection, secondary immune events likely aggravate COVID-19. Both publications underlying this dissertation investigated disease severity-related responses of macrophages or monocytes to SARS-CoV-2 to gain an understanding of detrimental host factors following infection with the newly emerged virus. Both studies followed a dual-cohort hypothesis-generating and validation framework.

In the first study of this dissertation, we investigated a total of 242 peripheral blood samples of 109 donors with mild or severe COVID-19, flu-like disease, or from healthy controls. Multiparametric technologies such as single-cell RNA sequencing (scRNA-seq) and Cytometry by time of flight (CyTOF) revealed monocyte responses distinctly differentiating severe and mild cases. While $CD14^{+}$/$HLADR^{hi}$/$CD83^{hi}$ monocytes marked flu-like disease and mild COVID-19, severe COVID-19 monocytes exhibited a $CD14^{+}$/$HLA-DR^{lo}$/$Calgranulin^{hi}$ phenotype. Hence, peripheral $CD14^{+}$ monocytes in severe COVID-19 exhibited lower levels of hallmarks of antigen presentation, antiviral response, and cyto-

kine-mediated inflammation. Additionally, we measured higher CD163 expression in severe and mild COVID-19 in comparison to controls and flu-like illness, which has been used as a marker for so-called “alternative” macrophage activation.

In the main study of this dissertation, we investigated pulmonary macrophage responses in 47 donors with COVID-19 acute respiratory distress syndrome (ARDS). $CD163^+$ macrophage numbers were increased in lung tissues of deceased COVID-19 patients, and broncho-alveolar lavage macrophage composition was dominated by $CD163^+$ macrophages that co-expressed LGMN macrophages (CD163/LGMN-Mφ) at early time points of the disease. Strikingly, CD163/LGMN-Mφ differentially expressed gene signatures of macrophage polarizations found in pulmonary fibrotic diseases, such as idiopathic pulmonary fibrosis (IPF). Accordingly, we found radiological, histological, and lung mechanical evidence of COVID-19-triggered pulmonary fibrosis. Here, we show that amongst other genes, LGMN and SPP1, but not CD163 activation, are central to fibrosis-associated gene signature enrichment.

We conducted *in-vitro* experiments to analyze the direct response of monocytes to SARS-CoV-2 (D614G index strain), employing functional single-cell transcriptomics and mass spectroscopic proteomics. SARS-CoV-2, but not Influenza A, induced the expression of the same fibrosis-associated gene sets. Furthermore, these monocyte responses differed from those after stimulation of inflammatory and antiviral immune receptors.

In summary, monocyte and macrophage phenotypes in severe COVID-19 of early variants were not characterized by the expression of prototypical antiviral genes, but by calgranulin and fibrosis-associated gene modules, respectively.

1 Introduction

The high lethality of Coronavirus Disease 2019 (COVID-19) during the 2020 pandemic waves brought the threat of infectious diseases to the broader public's attention. This dissertation aims to better understand COVID-19 pathology by analyzing monocyte and macrophage gene expression states.

In the healthy alveolus, the center stage of COVID-19 pneumonia, macrophages are the most abundant immune cell[1]. Moreover, monocyte-derived macrophages are rapid responders to infectious damage to tissue integrity[2]. Because of their general role as specialized tissue caretakers, macrophages express a particularly large variety of microenvironmental sensors[3]. Activation of these sensors induces downstream gene expression changes. Therefore, macrophage gene expression reflects the overall tissue processes surrounding these cells.

Moreover, inadequate polarization of macrophages has been widely attributed to aberrant or overshooting defense and repair processes[4]. In a first approximation, monocytes can be viewed as precursors of macrophages found in the blood. Accordingly, monocytes are easily accessible for lowly invasive diagnostics[5]. Therefore, the work underlying this dissertation aimed to describe how monocyte and macrophage gene expression states are associated with disease severity to gain a deeper understanding of COVID-19 lethality.

This dissertation presents multidimensional data published in two papers. In paper B of this dissertation, which was published first, we studied human monocyte phenotypes in the peripheral blood of mild and severe COVID-19 patients at single-cell resolution[6]. $CD14^{+}$ $HLA\text{-}DR^{hi}$ monocytes were elevated in mild COVID-19 and expressed higher levels of inflammatory and antiviral genes. Conversely, $CD14^{+}$ $HLA\text{-}DR^{lo}$ monocytes were elevated in severe COVID-19 and expressed the highest levels of calgranulin (S100A8/9/12). Both mild and severe COVID-19 cases expressed significantly higher levels of CD163 than controls.

In paper A of this dissertation, we investigated pulmonary macrophage-related immune responses in severe COVID-19 using scRNA-seq, single-nuclei RNA sequencing, and multiparametric microscopy. Furthermore, we investigated responses of primary monocytes to Severe Acute Respiratory Syndrome Corona Virus 2 (SARS-CoV-2) infection with scRNA-seq and mass-spectrometry (MS) based proteomics. We found fibrosis-associated macrophage signatures highly similar to fibrotic diseases such as idiopathic

pulmonary fibrosis. Remarkably, these phenotypes were directly inducible through the exposure of healthy primary human monocytes to SARS-CoV-2 *in vitro*. The studies underlying this synopsis generated detailed data on monocyte and macrophage responses to COVID-19. The results suggest a role of aberrant macrophage responses in COVID-19 pathology.

1.1 COVID-19 acute respiratory distress syndrome (ARDS)

In most patients, SARS-CoV-2 incites only mild to moderate respiratory disease. More than 5 % of hospitalized patients in Western demography, however, developed severe forms of disease with Acute Respiratory Distress Syndrome (ARDS) during the first wave of the pandemic [7–10]. As defined by the criteria of the Berlin definition, ARDS is a clinical syndrome of acute respiratory insufficiency. These criteria are: first, hypoxemia occurs within seven days after a known clinical insult or after the onset of new respiratory symptoms; second, respiratory failure is not fully explained by cardiac failure or volume overload; third, bilateral opacities are present in pulmonary radiography that are not entirely explainable by effusions, atelectasis, or nodules[11].

Pathologists approximate ARDS progression into two to three phases: A primary exudative stage characterized histopathologically by diffuse alveolar damage (DAD), followed by a fibroproliferative stage. Some patients progress to a third fibrotic stage.
Fibrosis is a pathological remodeling of tissues resulting in the non-functional replacement of functional tissue by connective tissue. Paper A of this dissertation was one of the first studies to describe fibrotic pulmonary disease induced by SARS-CoV-2 infection.

The remarkable efforts of the Recovery trial proved that aberrant immune responses are detrimental in severe COVID-19[12]. The glucocorticoid Dexamethasone, as well as the anti-inflammatory agents Tocilizumab, an anti-IL-6-antibody, and the JAK1/2-inhibitor Baricitinib, were shown to reduce the mortality of severe COVID-19[13–16]. However, anti-inflammatory therapy may not be specifically effective in ARDS caused by SARS-CoV-2. Dexamethasone has long been suggested as a potential therapeutic agent in ARDS of various causes. However, study sizes so far have been too small for sufficiently powered results[17,18]. Due to their central role in many pathological processes, macrophages could be involved in the efficacy of anti-inflammatory treatments for COVID-19 ARDS.

1.2 SARS-CoV-2

SARS-CoV-2 is a Betacoronavirus with approximately 80% sequence homology to SARS-CoV and correspondingly shares substantial proportions of protein sequences - including T cell epitopes - with endemic alpha and beta coronaviruses that are common causes of respiratory infections [19]. As previously shown, this similarity to HCoV-229E, -NL63, -OC43, and -HKU1 led to varying degrees of pre-pandemic cross-reactive T cell memory[20]. Nonetheless, the structure of the receptor-binding S1 region of the SARS-CoV-2 S protein is significantly altered compared to its endemic relatives. Therefore, pre-existing protective immunity of the adaptive immune system was minute at the population level[21]. Accordingly, SARS-CoV-2 met a world population with little specific immunity, leaving the initial anti-viral defense to innate immune cells such as macrophages[22].

1.3 Macrophages

Macrophages are innate immune cells, specialized as professional sentinels of tissue malfunction and pathogen-associated molecular patterns (PAMPS)[23]. Furthermore, they carry out supporting processes essential for many primary tissue functions[3]. For these tasks, they express a multitude of homeostatic receptors such as fatty acid sensing through PPARy, hypoxia sensing through HIF-1/2, or sensing of fragmented extracellular matrix (ECM) components after injury[24–27].

Loss of GM-CSF-guided alveolar macrophage differentiation results in alveolar proteinosis by accumulation of surfactant proteins in alveoli, exemplifying their critical role in pulmonary function[28].

1.3.1 Macrophage-induced pathology

Given their importance in many tissue and defense functions, it is not surprising that macrophages are involved in diverse pathologies. In viral pneumonia, for instance, the adoptive transfer of long-lived monocyte-derived macrophages of mice that had experienced influenza infection leads to increased lung damage after ensuing influenza infection in the recipient mice [29]. Furthermore, specific macrophage functions are involved in fibrosis progression. They induce TGFβ1 activity, fibroblast proliferation, extracellular matrix (ECM)

accumulation, epithelial-mesenchymal transition, and promote vascular remodeling and angiogenesis[30–32].

1.3.2 Monocytes and macrophages in inflammation

Blood monocytes, in the spotlight of paper B of this dissertation, differentiate into monocyte-derived macrophages or dendritic cells (mo-DC) after diapedesis into tissues[33]. Prototypically, CCL2 and CCL7 guide monocytes along their concentration gradients toward activated tissues by binding CCR2 - one of the most specific monocyte/macrophage markers[34,35].

After severe tissue infection, monocytes are promptly recruited in massive amounts into the bloodstream, typically from their bone marrow pool of storage and differentiation [36,37]. Cytokines such as IL-1β, G-CSF, and Interferon γ, released at sites of inflammation, alter the differentiation fate of multipotent progenitor cells towards a propensity for myeloid differentiation[37]. Exceptionally high cytokine levels during acute inflammation cause a massive increase in monocyte recruitment [38,39]. Hence, monocytosis is a long-established clinical indicator of systemic inflammation [40].

However, the diagnostic and prognostic value of detailed monocyte phenotypes for specific pathology, such as active viral defense, wound healing, fibroproliferation, and hyperinflammation, are likely underutilized. One of the aims of this dissertation was to contribute to deciphering such cellular states.

1.4 Relatedness of monocytes and pulmonary macrophages

Two long-standing macrophage and monocyte research paradigms were improved in the last decade. Firstly, this was the concept that tissue macrophages are replenished solely by bone marrow resident precursors, with monocytes being the necessary intermediate. Van Furth and colleagues first stated this model in 1968, and it remained the dominant perception of the relatedness of monocytes and macrophages for the following decades[5,41]. More recently, however, ample evidence has accumulated that tissue macrophages replenish in situ to varying degrees depending on inflammatory signaling and organ-specific factors[41–44].

The second central paradigm stated that macrophage phenotypes can be delineated by a handful of markers, directly allowing an inference of phenotypic function into either type 1 or type 2 (M1/M2) macrophages. This is now often viewed as having limited utility in explaining complex tissue processes[23,45–47]. The concept was adopted in analogy to T helper cell 1 and 2 subsets. However, in contrast to T helper cells, macrophage subset delineation is overlapping and diverse, especially in humans[45,46]. It is reasonable, however, to hypothesize that in health-promoting processes, some functions of macrophages, such as wound healing and tissue-destructing defense mechanisms, should not be active simultaneously[3,48]. Whether this is the case in human macrophages remains to be shown conclusively.

As a result of these paradigm shifts, monocyte/macrophage phenotypes can be understood as composites induced by specific microenvironmental requirements, cell-intrinsic functional programs, cell-cell interaction modules, and possibly stable differentiation states dependent on cellular ancestry[3,49,50]. Here, we aimed to support the effort of more complex descriptions of macrophage states and to uncover associations of monocyte and macrophage phenotypes to disease severity and fibrotic disease progression.

2 Methods

2.1 Publication B

2.1.1 Study design of publication B

To investigate differences in systemic immune responses, leukocytes of blood samples from COVID-19 patients were analyzed to delineate differences in mild and severe disease. Specimens of a total of 24 donors with mild (WHO ordinal scale 2-4) and 29 donors with severe COVID-19 (WHO ordinal scale 2-4) and 56 controls were analyzed by mass cytometry (CyTOF) droplet-based or microwell-based scRNA-seq and multi-color flow cytometry. The analytical focus was set on myeloid cells.

2.1.2 Cohort 1 - Berlin cohort

Heparinized whole blood was drawn, and processing started within 4 hours. PBMCs were isolated from whole blood using density gradient centrifugation with 1,077 g/ml Pancoll. Erythrocytes were removed by negative selection with CD235a magnetic beads separation (BD). PBMC patient samples were hashtagged with TotalSeq-A antibodies (BioLegend), following the manufacturer's protocol for use with 10x Single Cell 30 Reagent Kit v3.1.

2.1.3 Cohort 2 - Bonn cohort

Please refer to the original publication for a thorough method description of cohort 2. In the Bonn cohort, scRNA-seq was performed on EDTA or heparin fresh whole blood, fresh PBMC, and frozen PBMC. Analysis methods included scRNA-seq (BD Rhapsody, 10x Chromium) and multi-color flow cytometry (MCFC).

2.1.4 Single-cell library generation and sequencing

The cell suspension was super-loaded into the Chromium Controller at 50,000 cells/ml concentration. Reverse transcription, cDNA amplification, and library construction were conducted following the protocol provided by 10x Genomics with the single cell 3’ reagent

kit v3.1. The hashtag libraries were prepared according to the cell hashing protocol for 10x Single Cell 30 Reagent Kit v3.1 from BioLegend, using the specified primers and reagents. The libraries were quantified using a QubitTM 2.0 Fluorometer from ThermoFisher and checked for quality with an Agilent 2100 Bioanalyzer and High Sensitivity DNA kit. The libraries were sequenced in paired-end mode on an Illumina NovaSeq 6000 sequencer with S1 and S2 flow cells, using 50 cycles.

2.1.5 Data preprocessing

The scRNA-seq data from the 10x Genomics Chromium platform were pre-processed using CellRanger v3.1.0. A digital gene expression (DGE) matrix was created for each sample by mapping the reads to a reference genome that included both the GRCh38 genome and the SARS-CoV-2 genome. The number of unique molecular identifiers (UMIs) for each gene in each cell was recorded in the DGE matrix.

CellRanger output was analyzed in R 3.6.2 using the Seurat package version 3.1.4. The UMI count matrices were demultiplexed using the HTODemux function in Seurat. Quality control measures were applied, excluding cells with 25% mitochondrial reads, more than 25% HBA/HBB gene reads, fewer than 250 or more than 5,000 expressed genes, and fewer than 500 detected transcripts. Genes that were expressed in fewer than five cells were also excluded from the analysis. After log-normalization and scaling, principal component analysis (PCA) was performed on the 2,000 most variable features (vst, Seurat). The first 20 PCs were integrated with publicly available scRNA-seq data from healthy controls using the harmony algorithm[51]. Control data was taken from Reyes et al.,2020[52], 10x v3.1 PBMC benchmarking data from healthy controls, and 10x v3.1 scRNA-seq data from the first cohort and filtered using the quality criteria described above.

2.1.6 Cluster analysis

Two-dimensional UMAP based on the 20 first dimensions of the harmony data Louvain clustering algorithm with a resolution of 0.4 was employed for data segregation. Cell-level DEG was aided by the Wilcoxon Rank Sum test, and genes with log-fold changes greater

than 0.25, at least 25% expressed in the tested groups, and Bonferroni-corrected p-values less than 0.05 were considered DEGs. Cluster marker genes represent testing of the respective cluster versus all other clusters.

2.2 Publication A

2.2.1 Study design of publication A

Bronchoalveolar lavage and tissue samples were obtained from 47 patients suffering from COVID-19 ARDS. Specimens were analyzed using single-cell RNA-Sequencing (scRNA-seq) and single-nucleus RNA-sequencing (snRNA-seq), immunofluorescence (IF) microscopy, multi-epitope ligand cartography (MELC), immunohistochemistry (IHC), RNA-fluorescence in situ hybridization (RNA-FISH), and transmission electron microscopy (EM). Clinical data included lung mechanics and computed tomography (CT) imaging. While outcomes were either hospital discharge or death, time courses were diverse, ranging from death five days to 223 days after symptom onset.

2.2.2 Cohort 1 - Berlin, ICU cohort

Patients with COVID-19-associated ARDS treated at a single intensive care unit (ICU) between March 17, 2020, and March 17, 2021 were included. These patients were part of the Pa-COVID-19 study, a pathophysiology and clinical characteristics research project of COVID-19 patients at Charité Universitätsmedizin Berlin. The study was approved by the Institutional Review Board of Charité, and written informed consent was obtained from all patients or their legal representatives. The patients included in the assessment of CT images and pulmonary gas exchange required veno-venous extracorporeal membrane oxygenation (vvECMO) treatment. Out of 18 identified patients, two were excluded from the analysis due to death within 36 hours of vvECMO initiation. Information on the age, sex, medication, comorbidities, and outcome of these patients is provided in Wendisch,… et al., 2021.

2.2.3 Cohort 1 - Berlin, pathology cohort

The autopsy study was approved by the Ethics Committee of the Charité Universitätsmedizin Berlin and was conducted according to the Declaration of Helsinki. For this study, we analyzed cryopreserved lung tissue from deceased patients with COVID-19. The patients included in this study were selected from an autopsy cohort at Charité and met the inclusion criteria of having cryopreserved material and detectable levels of SARS-CoV-2 RNA in the lung tissue. Patients with detectable tumor infiltration or a graft-versus-host reaction after stem cell therapy were excluded from the analysis. Information on the age, sex, medication, and comorbidities of these patients is listed in paper A, Table S1.

2.2.4 Cohort 2 – Aachen

The Aachen cohort includes 15 consecutive autopsies of COVID-19, SARS-Cov-2 positive patients between March 9, 2020 and January 1, 2021. The study was approved by the local ethics committee. All patients were tested positively for SARS-CoV-2 with at least one PCR test from respiratory samples in a clinical setting before the autopsy. Consent for the autopsy was obtained from the legal representatives of the deceased patients. The autopsy protocol was developed for increased employee safety and optimization of sample acquisition as part of the German Registry of COVID-19 autopsies (DeReg-COVID). Five non-COVID clinical autopsy lung tissues sampled between 2013 and 2015 were included as controls in this cohort. Additionally, one clinical biopsy tissue sample from a COVID-19-positive patient and two non-autopsy biopsy samples of lung tissues from non-COVID-19 surgical patients were incorporated into the histological survey.

2.2.5 Additional datasets for data integration

Additional datasets were incorporated to perform data integration. The BAL scRNA-seq macrophage data from this study were combined with data from three previously published datasets. For Pulmonary fibrosis: Adams et al. (GSE136831), Morse et al. (GSE128033); for a COVID-19 Bharat et al. (GSE158127)[53–55]. The fibrosis studies are outlined in **Table 1**. Detailed cohort descriptions can be found in the original publications.

2.2.6 Histological analysis

For histological analysis, paraffin-embedded tissue samples were cut into 1mm thick sections, deparaffinized, rehydrated, and stained with hematoxylin-eosin (H&E). The samples were taken from the central and peripheral parts of each lobe and were fixed in 4% formaldehyde. The staining was automated (Tissue-Tek Prisma Plus & Tissue-Tek Film) according to the provided protocols. For immunohistochemistry (collagens I, III, IV, CD68), 1 mm thin FFPE sections were stained according to a previously published detailed protocol[56].

Macrophage subtypes were analyzed with the VECTRA automated quantitative pathology imaging system according to the pre-established protocol[56].

Ashcroft scoring was applied to samples of cohort 2. Fields of the tissue that were predominantly occupied by large bronchi or vessels or by malignant tumor deposits were not included in the scoring. The scores were determined independently by two experienced pathologists, and the mean value of the two scores is reported. Briefly, RNA-FISH was conducted on 1 mm thin FFPE sections with the RNAscope Multiplex Fluorescent Reagent Kit v2 assay (Advanced CellDiagnostics, Inc., Hayward, USA). Wilcoxon Rank-Sum Test at the significance level of 0.05 is indicated.

2.2.7 Multi-epitope ligand cartography

Multi-epitope ligand cartography (MELC) image acquisition was performed as previously described[57,58]. The multiplexed histology data was generated using a modified Toponome Image Cycler MM3 (TIC, MelTe). MELC runs consist of a series of cycles, each of which includes the following four steps: staining with a fluorescence-coupled antibody and washing; auto-focused image acquisition of a fluorescence image 3D stack; photobleaching; and lastly, a second auto-focused z-stack image acquisition. Each staining included a combination of PE, FITC fluorophores, and DAPI.

The images were automatically overlaid by cross-correlation with the reference phase contrast image. Background and illumination were corrected by reference to the bleached images after each cycle[59]. To account for slice thickness, an 'Extended Depth of Field' algorithm was applied to the 3D fluorescence stack in each cycle (Pertuz et al., 2013). Normalization was conducted with Fiji[60]. After rolling ball algorithm background

estimation and edge removal, fluorescence intensities were adjusted to the full image bit range. Segmentation and subsequent analysis of the obtained 2D images was conducted with CellProfiler 3.1.8.

The mean fluorescence of individual cells was hyperbolic arcsine transformed and imported into R version 3.6.3. The entire panel contained 22 markers. Normalized and scaled values were used to compute a 2D UMAP embedding with the R package “uwot”[61]. All CD45-expressing cells were selected for Louvain clustering. Cells were identified by literature-informed standard markers.

2.2.8 Clinical investigation

The clinical investigation included the measurement of inspiratory vital capacity (VCin) and CT scans. VCin was measured using an automated inspiratory/expiratory pressure-volume curve on a ventilator (S1, Hamilton Medical). The pressure was increased in 2 mbar/second increments from 0 to 45 mbar followed by release back to 0 mbar. The volume of the lungs at 45 mbar was interpreted as VCin. All measurements were performed while the patients were under deep sedation in a supine position to prevent spontaneous breathing. For patients with available VCin measurements, five individuals, the highest VCin during the early phase of vvECMO support and the lowest during the later phase (> seven days of vvECMO support) were compared.

CT scans were performed in the supine position. When clinically feasible, one CT scan was acquired within seven days after ICU admission and around the time of vvECMO initiation. Lastly, the last available scan was included.

2.2.9 BAL macrophage scRNA-seq cell library generation

BAL samples were collected from mechanically ventilated COVID-19 patients. After erythrocytes lysis with red blood cell lysis buffer (BioLegend), a total of 16,500 cells were loaded into the 10x Genomics Chromium controller. Libraries were processed separately according to the reagent kit v3.1 by 10x Genomics. The libraries were quantified and quality-checked using the QubitTM 2.0 Fluorometer (ThermoFisher) and the 2100 Bioan-

alyzer with the High Sensitivity DNA kit (Agilent). Paired-end mode sequencing was performed with S1 and S2 flow cells (2 3 50 cycles kit) on the NovaSeq 6000 sequencer (Illumina).

2.2.10 BAL data analysis

CellRanger output files were imported into R, and low-quality transcriptomes were filtered out. Data was processed with the R library Seurat[62]. Data was normalized and scaled. A dimensional reduction was computed using the RunPCA function based on the highly variable genes, and the FastMNN algorithm was applied to account for the batch effect observed by sample[63]. UMAP was used to visualize the resulting data in two dimensions. Clustering was performed using the Louvain algorithm with a resolution of 0.4. Clusters were annotated with cell types using literature-based markers. For analysis of the monocyte/macrophage compartment, cells in the relevant clusters were subsetted and basic steps such as normalization, scaling, and dimensional reduction were repeated, along with Louvain clustering with a resolution of 1.5. The resulting clusters were annotated as monocyte/macrophage subtypes based on previously identified markers. Cell-level DGE analysis was aided by the one-sided Wilcoxon rank sum test. The "block" argument was used for patients in the BAL dataset.

Using the gene sets indicated in **Table 1**, we calculated module scores per cell. Cell-level Wilcoxon rank sum test with blocking for sample factor was used to aid in the identification of differences. Here, a population-level analysis is amended. Module scores were added for all cells in each donor-cluster group. Effect size was determined by Cohen's d relating mean differences (sample vs. rest) to group and total variance. Significance was determined by T-test at a 0.05 significance level with Benjamini Hochberg correction incorporating the first and second highest scored groups. Indicated genes are ranked by calculating the largest influence on effect size in a leave-one-out method.

2.2.11 Data integration and proximity metric

The number of cells from Adams was downsampled to balance the number of cells in each category (IPF, control, and COPD). Single-cell variational inference (scVI) was used to integrate pulmonary single-cell transcriptomes from three previous studies (Adams et

al., Morse et al., and Bharat et al.) using patient and sample identifiers as batch covariates53–55. The resulting latent representation was used to compute k-nearest neighbor and UMAP graphs using SCANPY[64].

The 15 nearest neighbors to a cell were determined by Euclidean distance in the integrated gene space, followed by a majority voting by neighbor origin (fibrosis/healthy control) to assess the proximity of cells of the different conditions. We repeated this procedure with each COVID-19 dataset separately to ensure the independence of these analyses. Statistical significance of proximity ratios was determined for each cell type by Fisher's exact test with Benjamini Hochberg correction at a 0.05 significance level.

2.2.12 Viral stocks

A passage 0 SARS-CoV-2 sample (BetaCoV/Munich/BavPat1/2020 EPI_ISL_406862 strain, (GISAID accession: EPI_ISL_406862) was incubated at 37°C and 5% CO2 on approximately 1x10e6 VeroE6 cells. After three days, the virus-containing supernatant was filtered with centrifugal filters (Vivaspin 100 kDa MWCO, GE Healthcare). Importantly, the absence of any second-site mutations was confirmed by next-generation sequencing.

Influenza A/Panama/2007/1999 virus (IAV) was cultured in MDCKII at a multiplicity of infection (MOI) of 0.01. The virus-containing supernatant was then centrifuged for 5 minutes at 3500 rpm. Virus titers were determined using standard plaque titration assay with VeroE6 (SARS-CoV-2) or MDCKII cells (IAV) with Avicel overlay. Virus stocks were stored at -80°C."

2.2.13 Monocyte Isolation and in-vitro stimulation

PBMCs of healthy donors were isolated from fresh EDTA blood or buffy coats using gradient centrifugation (1.077 g/ml Pancoll, PAN Biotech). The pellet was then subjected to immunomagnetic depletion of cells expressing CD3, CD19, CD20, CD56, or CD235a using biotinylated antibodies (Biolegend) coupled to MagniSort Streptavidin Negative Selection Beads (Invitrogen). Classical monocytes were sorted with a BD FACS Aria SORP cell sorter (BD Biosciences) as HLA-DR+/CD14+ and negative or low for CD3, CD19, CD20, CD56, CD16, CD141, CD304 and CD1c.

For scRNA-seq experiments, 1x10e5 cells per well were plated in a 96-well format, while for proteomics experiments, 1x10e6 cells/well were given into a 12-well plate. Cells were rested for one hour at 37°C and 5% CO2. For scRNA-seq experiments, the concentrated SARS-CoV-2 isolate was added at a multiplicity of infection (MOI)) of 5, and the total volume was adjusted to 100 µl. For proteomic experiments, SARS-CoV-2 and Influenza A were added at MOI of 30 and 10, respectively, in a total volume of 1.5 ml. For scRNA-seq experiments, R848 (InvivoGen) and pre-complexed 3p-hpRNA (LyoVec) were added at a final concentration of 1.2 ug/ml and 16 ng/ml, respectively, to separate wells. After incubation, cells were detached carefully with ice-cold 10mM EDTA in PBS at 16 hours for the scRNA-seq experiments or 1 hour, 3 hours, and 18 hours in the MS proteomics experiments.

2.2.14 Analysis of in-vitro scRNA-seq data

Library preparation and data preprocessing were conducted as stated above with thresholds and filter variations as in paper A, table S3. Donors were demultiplexed by donor polymorphisms using the Souporcell algorithm[65]. Marker genes were selected by cell-level Wilcoxon rank sum test p-value and fold change blocked for donors. Module scores were calculated as in the BAL data with the same reference gene sets.

2.2.15 Proteomic analysis of in-vitro stimulated monocytes

Proteomics samples were prepared using a method adapted from Mertins et al.[66] In brief, the samples were pre-treated with LysC and digested with trypsin. Peptides were randomly assigned to TMTpro channels and labeled with TMTpro reagents. For total proteome analysis, the MS was set to data-dependent acquisition mode. The 20 most intense precursor ion peaks with charges from +2 to +6 were selected for fragmentation unless present in the dynamic exclusion list. RAW files were analyzed with MaxQuant v1.6.10.4367. TMTpro was manually set as a fixed modification/quantification method. An ANOVA test was used to identify significant differences, and the results were corrected for multiple comparisons using the Benjamini-Hochberg method. Proteins that showed significant differences were then clustered using fuzzy-c-means clustering and analyzed for enrichment of gene sets using the GSEA suite and the MSigDB database. P values

(one-sided Wilcoxon signed-rank test) are reported for the enrichment of the indicated reference gene sets calculated by eCDF.

3 Results

3.1 Analysis of peripheral blood monocytes in severe and mild COVID-19 - Publication B

To gain insight into disease severity-related immune responses, we comparatively investigated peripheral immune cell activation and composition of patients with mild and severe COVID-19. In a two-cohort study, we employed scRNA-seq and CyTOF on 242 peripheral leukocyte or PBMC specimens of 109 individuals (**Fig. 1A/B**). The two-cohort design served as a discovery and validation framework. Differences between mild and severe COVID-19 were most prominent in myeloid cells. Here, a summary of the results of the monocyte compartment with a focus on cohort 1 is presented.

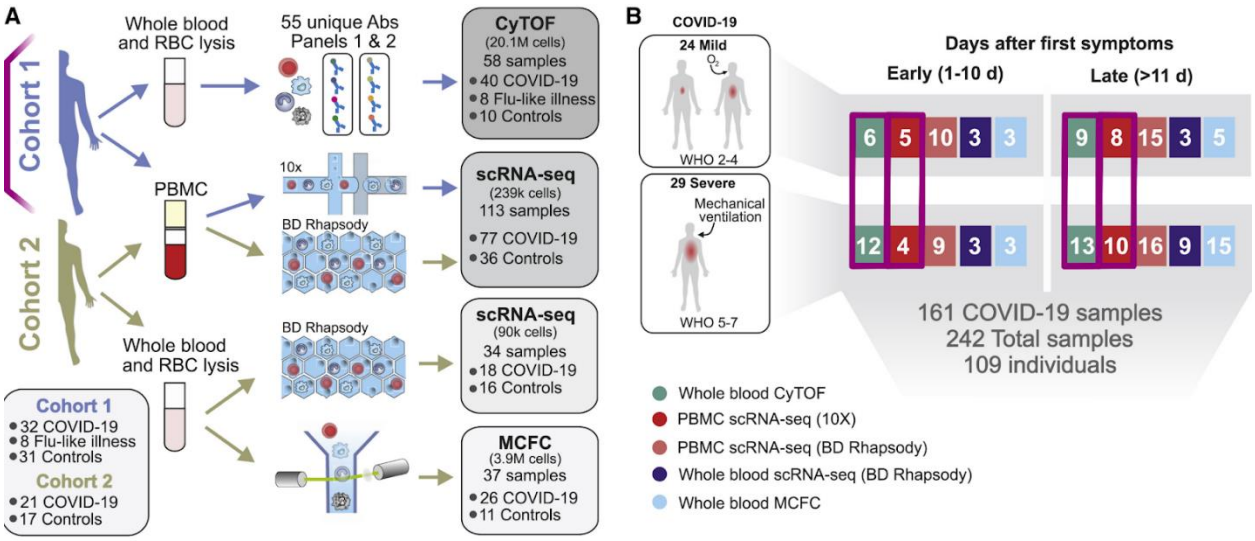

Figure 1: Study design publication B [Schulte-Schrepping,..., Wendisch et al.].

(A) Sampling overview of control and COVID-19 peripheral leukocyte samples of the two cohorts. Data from Cohort 1 that is elaborated in this synopsis is indicated by purple identifiers. Peripheral Blood Mononuclear Cells (PBMC) were pelleted from EDTA-treated peripheral blood with density gradient centrifugation before library preparation with the 10x Chromium protocol or CyTOF mass cytometry. Whole blood after red blood cell lysis was analyzed with multi-color flow cytometry (MCFC) and or scRNA-seq (BD Rhapsody). [modified from Schulte-Schrepping,..., Wendisch et al. 2020] (**B)** Number of samples according to disease severity and time point analyzed with each technique of A. [modified from Schulte-Schrepping,..., Wendisch et al. 2020]

3.1.1 Identification of monocyte phenotypes associated with disease severity

Deploying CyTOF and FACS, we detected, on average, a neutrophil-dominated leukocytosis in patients with severe COVID-19. Non-classical monocyte frequencies were significantly diminished in COVID-19 versus control but not in Flu-like illness. Overall monocyte counts in COVID-19 samples were more varied without a significantly altered central tendency (**Fig. 2A)**. Hierarchical clustering of CyTOF intensities of 39 markers in monocytes and dendritic cells revealed high expression of $CD226^{+}$ and $CD69^{+}$ concomitant with a $HLADR^{lo}/CD11c^{hi}$ phenotype in monocytes, particularly in severe COVID-19 (**Fig. 2B/C)**. CD69 is a cell surface lectin that is induced by TGF-beta in a SMAD3-dependent manner[68]. Physiologically, TGF-beta restricts excessive immune responsiveness and induces tissue regeneration[69]. CD226 facilitates monocyte transendothelial migration. Hence, this monocyte population may constitute an extravasation-ready macrophage precursor with immune-curtailing functions[70].

For a higher cell-level resolution, we conducted scRNA-seq on PBMC samples. Starting with the very first COVID-19 patients of our center, we sampled 27 specimens from 18 COVID-19 patients (8 mild,10 severe) between day three and day 20 after symptom onset. Next to CD4 T cells, myeloid cells showed the most prominent segregation in Louvain clustering and UMAP projection between mild and severe COVID-19 (paper B, Fig. 2A, 2B, 2D; **Fig. 2D/E**).

We investigated the monocyte clusters in further detail and identified 4 clusters with attributable biological relevance. A fifth cluster was almost exclusively composed of cells of a single sample and is left out here for a more conservative analysis. The differential gene expression of CD14 in clusters 0,1 and 3, as well as CD16 (FCGR3A) and CX3CR3 in cluster 4, allowed us to identify these clusters as classical and non-classical monocytes, respectively (**Fig. 2D/G**). Predominantly, cells of mild COVID-19 samples segregated from inactivated classical monocytes and were marked by high expression of CD83 (cluster 1), a salient co-stimulatory molecule for inflammatory antigen presentation (**Fig. 2E/F**). These cells also exhibited high levels of interferon-inducible transcripts (e.g. IFI27, IFI44L) and central mediators of inflammation such as Interleukin 1 beta (IL1B) and interferon regulatory factor 1 (IRF1). A separate cluster with maximum counts of calgranulin transcripts (S100A8/A9/A12) expressed comparatively faint levels of MHC II transcripts (e.g. HLA-DRA/HLA-DRB1) (cluster 3). This cluster was vastly dominated by samples from severe cases (**Fig. 2E/F**). Reassuringly, data from cohort 2 supported these

results. Monocytes of both COVID-19 groups exhibited higher levels of CD163 with excess zeros typical of scRNA-seq data[71]. CD163^{hi} monocytes clustered separately in cohort 2. CD163 is a hem/haptoglobin complex scavenger receptor. (**Fig. 2H)**[72,73]. A low expression of markers of inflammation, antigen-presentation and viral defense characterized, all in all, monocytes in severe COVID-19.

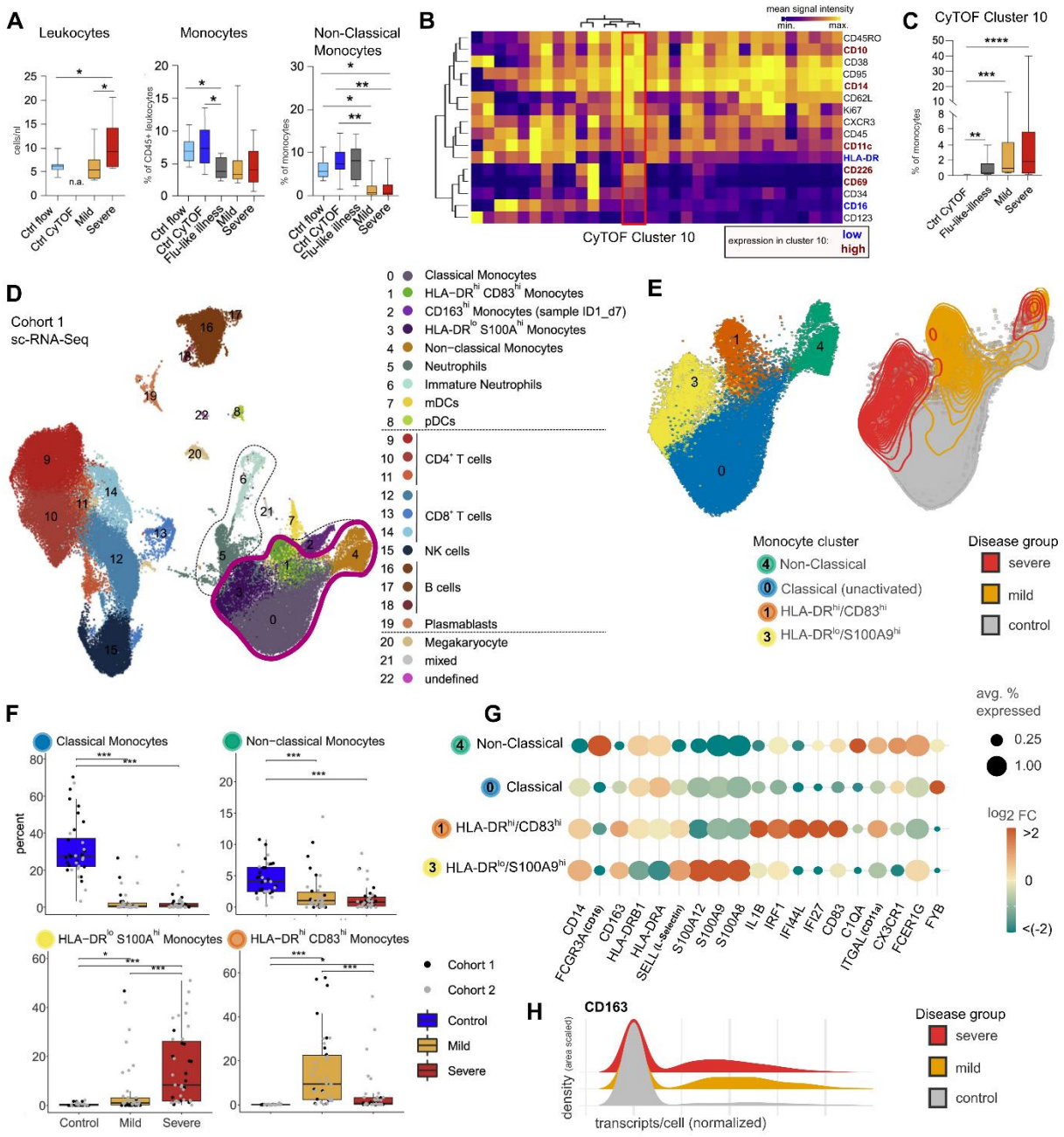

Figure 2: Differences in monocyte polarization between mild and severe COVID-19.

(A) Box and whisker plots illustrating cell lineage composition measured with CyTOF from whole blood of COVID-19 patients with mild (n = 8) or severe disease (n = 9), Flu-like illness (n = 8), and age-matched controls with additional FACS controls (ctrl CyTOF, n = 9, ctrl; flow, n = 19, Kverneland et al. (2016)). Kruskal-Wallis and Dunn's test gave the result of significant group differences (∗p < 0.05, ∗∗p < 0.01, ∗∗∗p < 0.001, ∗∗∗∗p < 0.0001). Not available data is indicated by "n.a.". [adapted from Schulte-Schrepping,..., Wendisch et al., 2020] **(B)** Heatmap of CyTOF data of cohort 1 monocytes and DCs of whole blood samples from mild (n = 8) and severe (n=9)

COVID-19, controls (n=9), and Flu-like illness (n=8). Columns depict hierarchical clusters of cell-wise intensity measurements of 39 markers. Rows depict the most discriminatory markers. Partial cluster tree for clusters with closest Euclidean distance to cluster 10. The expression of relative marker intensities for cluster 10 is color-coded. Abundance testing via generalized mixed effects models and multiple comparison adjustments using the Benjamini-Hochberg procedure and a false discovery rate (FDR) cutoff of 5% across all clusters/subsets and between-group comparisons. [modified from Schulte-Schrepping,..., Wendisch et al., 2020] (**C)** Box and whisker plots (quartiles 2 & 3, 10–90 percentile) of monocyte clusters 10 from (A). Abundance testing via generalized mixed effects models and multiple comparison adjustment using the Benjamini-Hochberg procedure counting clusters/subsets and between-group comparisons (∗p < 0.05, ∗∗p < 0.01, ∗∗∗p < 0.001, ∗∗∗∗p < 0.0001). [from Schulte-Schrepping,..., Wendisch et al., 2020] (**D)** Integrated scRNA-seq UMAP of 99,049 Leukocytes from 49 samples (8 mild, 10 severe patients) and 22 control. Colors according to Louvain clustering cell type classification. [modified from Schulte-Schrepping,..., Wendisch et al., 2020] **(E)** Integrated scRNA-seq UMAP of multi-donor monocyte clusters from **(D)**(48,266 monocytes) colored according to Louvian cluster classification based on marker-gene-guided reference-based annotation (left). Density distribution is depicted by density lines of cells from samples according to disease severity (right). For clarity, a cluster mainly consisting of a single specimen was excluded from the depiction due to a high probability of it being an artifact and of limited informative value. [original figure with data from Schulte-Schrepping,..., Wendisch et al.,2020] **(F)** Box (quartile 2&3) and whisker plots of per-patient frequencies of PBMC subsets. Color coding of boxes according to disease severity; data points color according to cohort. Joint differential abundance testing with Dirichlet-multinomial regression adjusted with the Benjamini-Hochberg method, *p < 0.05, **p < 0.01, ***p < 0.001. [adapted from Schulte-Schrepping,..., Wendisch et al., 2020] **(G)** Dot plot of selected highly significant (cell-level) literature informed marker genes indicating monocyte subset differences. [original figure with data from Schulte-Schrepping,..., Wendisch et al., 2020] (**H)** Area-scaled density of CD163 normalized cell counts by disease groups (Gaussian kernel) [original figure with data from Schulte-Schrepping,..., Wendisch et al.,2020]

3.2 Analysis of pulmonary macrophages in severe COVID-19 and monocyte responses to SARS-CoV-2 - Publication B

In the main study of this dissertation, we sought to characterize macrophage-related processes that occur in the lungs of patients with severe COVID-19. To this end, we collected tissue samples and bronchoalveolar lavage cell samples from 47 patients diagnosed with COVID-19 ARDS. These samples were subjected to multiple analytical techniques, including scRNA-seq, MELC, immunofluorescence microscopy, immunohistochemistry, RNA-fluorescence in situ hybridization, and transmission electron microscopy focusing on macrophages. In addition, we investigated patients clinically with lung mechanics assessments and CT imaging (**Fig. 3**).

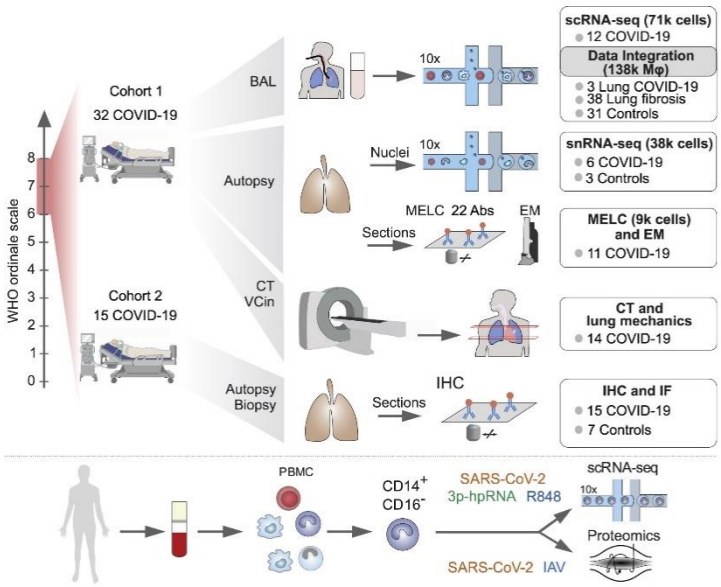

Figure 3: Study outline of publication A (2021).

[adapted from Wendisch et al.,2021], CT, computed tomography; BAL, bronchoalveolar lavage; scRNA-seq, single-cell RNA sequencing; snRNA-seq,single-nucleus RNA sequencing; IHC, immunohistochemistry; IF, immunofluorescence microscopy; MELC, multiepitope ligand cartography; EM, electron; microscopy; VCin, inspiratory vital capacity; PBMC, peripheral blood mononuclear cells; IAV, Influenza A virus.

3.2.1 Multiepitope immunofluorescence of autopsy lung tissue sections unveils an accumulation of CD163^{+} macrophages

Next, we analyzed lung autopsy tissue samples of nine donors who died of COVID-19, with MELC employing a panel of 22 markers. Three fields of view (FOV) per donor were scanned, of which 22 passed quality thresholds **(Fig. 4A/B/C)**. Following automated cell segregation, mean per-cell marker fluorescence was determined. Monocytes and macrophages could be delineated by UMAP dimensionality reduction and Louvain clustering **(Fig. 4C)**. Notable was a large percentage of macrophages expressing high levels of CD163 **(Fig. 4D)**. Conventional immunofluorescence microscopy of samples confirmed an increased fraction of CD163^{+} macrophages and a higher density of total macrophages in COVID-19 samples compared to healthy controls **(Fig. 4E/F)**.

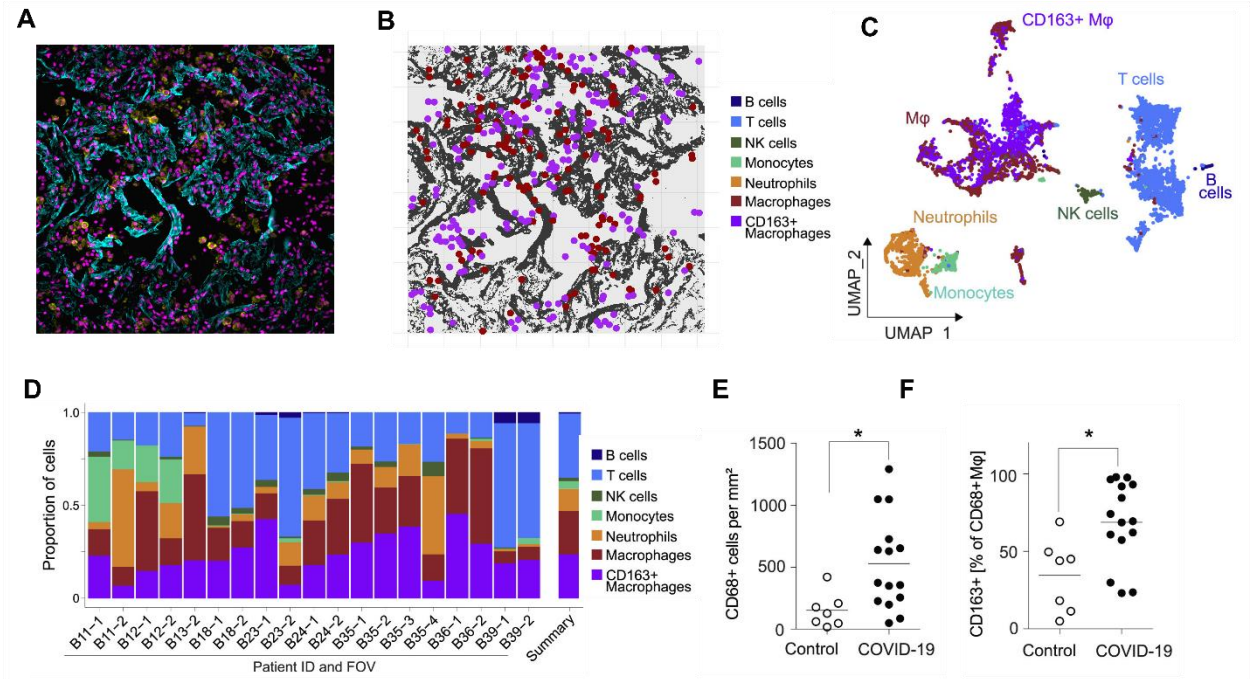

Figure 4: COVID-19 lung tissue samples reveal an accumulation of CD163+ macrophages

(A) Exemplary immunofluorescence field of view of autopsy lung tissue underlying the multi-epitope ligand cartography with 22 markers. Accumulation of Collagen IV (Cyan), CD163 (yellow), nuclear DNA stained with DAPI (magenta). [original figure with data from Wendisch et al.,2021] **(B)** Processed image data of (A) showing only the center of mass of macrophages after cell segregation and grey-scale Collagen IV staining. CD163-expressing macrophages marked by purple color. [original figure with data from Wendisch et al.,2021] **(C)** UMAP embedding and Louvain clustering of Multi-epitope Ligand Cartography imaging data of 9,684 CD45^{+} cells from lung autopsy samples of 9 COVID-19 patients. 22 markers and 22 fields of view, cohort 1. [apopted from Wendisch et al., 2021] **(D)** Cell type proportions of total CD45+ cells per fields of view for cells from (A) with annotated mean cell numbers. [adapted from Wendisch et al., 2021] **(E)** Immunofluorescence microscopy derived CD68+ macrophage density in lung autopsy samples from fifteen donors from cohort 1. Mann-Whitney u-test; *p < 0.05. [adapted from Wendisch et al.,2021] **(F)** Percentage of CD163+ Macrophages amongst all macrophages of (E). Mann-Whitney u-test; *p < 0.05. [adapted from Wendisch et al.,2021]

3.2.2 Single-cell transcriptome analysis of BAL macrophages

To gain deeper insight into the active processes of lung macrophages of patients with severe COVID-19, we analyzed BAL cells of samples from 12 donors with COVID-19 ARDS from day 7 to day 98 after symptom onset, with scRNA-seq. Macrophages were present at high percentages, albeit with transcriptomic differences to steady-state alveolar macrophages (paper A Fig.2A/S2E). To investigate this heterogeneity further, we integrated monocyte and macrophage transcriptomes separately by mutual nearest neighbor correction **(Fig. 5A)**[63].

We identified three neighboring clusters as subgroups of FABP4-positive conventional alveolar macrophages (AM), defined as AM1, AM2, and proliferating AM (**Fig. 5A/5C**).

Differential expression of monocyte markers such as CD14, Ficolin-1 and very high expression of S100 family proteins (S100A8, S100A9, S100A1) was seen in the cluster

on the far pole of the embedding, which we named FCN-1-Monocytes (FCN1-Mono) **(Fig. 5A/D)**. Cells characterized by high gene expression of CD163 and the asparaginyl endopeptidase Legumain (LGMN) clustered on a third pole of the UMAP embedding (LGMN/CD163-Mφ) **(Fig. 5A/5C)**. An intermediate cluster expressed an overlap of macrophage and monocyte markers (Mono/Mφ). LGMN/CD163-Mφ were upregulated during the peak of infection, although an inflammatory profile did not characterize this cluster. In contrast, LGMN/CD163-Mφ showed a predominant expression of tissue damage repair and proliferative transcripts **(Fig. 5C)**. Conventional AM signatures were prominent at later time points **(Fig. 5B)**.

Transcription Factor Target Over-representation Analysis, with the chromatin immunoprecipitation-X Enrichment Analysis 3 (CHEA3) tool, based on differentially expressed genes of the identified clusters predicted, PPARγ, a regulator of fatty-acid metabolization, as one of the most highly differentially expressed TFs in conventional AMs. Interestingly, transcription factors GLMP and TFEC, which are understudied in macrophages, were predicted to regulate the CD163/LGMN phenotype **(Fig. 5C)**.

In conclusion, scRNA-seq of BAL macrophages unveiled an accumulation of LGMN/CD163-Mφ in the first weeks of severe COVID-19, characterized by genes associated with tissue remodeling.

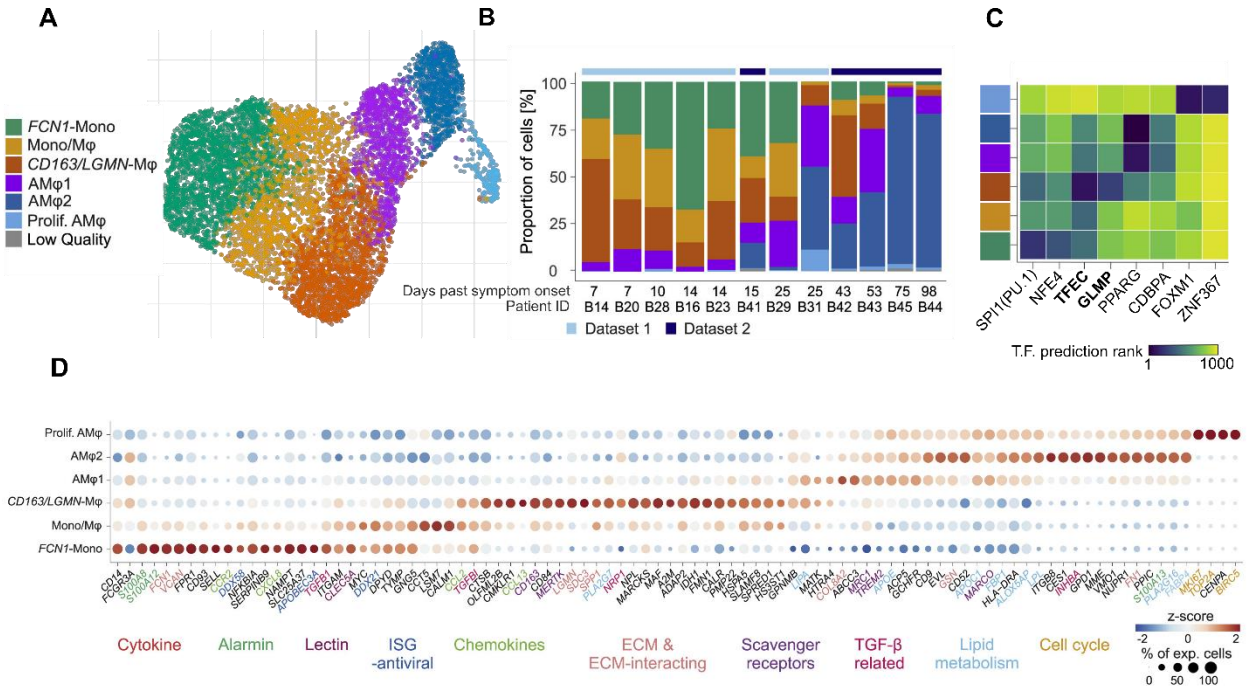

Figure 5: BAL macrophage single cell transcriptomes of COVID-19 ARDS patients.

(A) UMAP embedding of the first 15 multiple nearest neighbor integrated principle components of scRNA-seq of BAL macrophages from cohort 1 [adapted from Wendisch,... et al., 2021] **(B)** Proportions of clusters indicated in (A) by time after symptom onset [adapted from Wendisch,... et al., 2021] **(C)** Top two predicted transcription factors per cluster. Transcription factor target over-representation analysis based on differentially expressed genes of the clusters. The mean rank of ChIP-X Enrichment Analysis 3 (CHEA3)[74]-prediction based on Chip-Seq data displayed by the color gradient. Rank 1 refers to the highest prediction score. [modified from Wendisch,... et al., 2021] **(D)** Dotplot indicating z-score of average normalized gene counts respective to BAL macrophage cluster and percentage of cells per cluster in which the gene was measured. Literature informed the grouping of genes indicated by color. [adapted from Wendisch,... et al., 2021 (Mφ:Macrophage)

3.2.3 Evidence of fibroproliferative disease in COVID-19

Due to accumulating anecdotal evidence of fibrotic disease progression of COVID-19, we systematically compared the first and last available chest CT scans of 14 patients with COVID-19 ARDS (Paper A Fig. S5C, **Fig. 6A**). At early time points during the first two weeks after symptom onset, according to the Berlin definition of ARDS, multilocular bilateral ground glass opacities were present in all available CT scans. Later scans revealed progressive consolidation and reticulations indicative of fibroproliferative disease with an accumulation of cases suffering from pronounced fibrosis, as exemplified in **Figure 6A**. Fibrotic processes lead to reduced tissue compliance, which causes restrictive pulmonary disease. The radiological findings, therefore, prompted us to assess lung-mechanical alterations. To this end, we analyzed the inspiratory vital capacity (VC_{in}) at 45 mBar ventilatory pressure in a cohort of 16 patients suffering from COVID-19 ARDS requiring veno-venous ECMO treatment. All patients received lung-protective mechanical ventilation.

Median trough VC_{in} during ECMO treatment was significantly reduced compared to values at ECMO initiation, indicating a restrictive pulmonary deficiency compatible with fibroproliferative disease (**Fig. 6B**).

To assess fibrotic processes at the tissue level, we analyzed 14 autopsy samples and one biopsy from 15 patients with COVID-19 ARDS and seven non-COVID-19 controls from five autopsies and two biopsies. Histopathological evaluation indicated widespread tissue remodeling with excessive collagen deposition and loss of primary tissue structures (**Fig. 6C**). Histological assessment by two independent, experienced pathologists using the Ashcroft fibrosis score yielded significant fibrotic tissue alterations in COVID-19 tissues compared to controls (**Fig 6D**). In conclusion, we found ventilatory, radiological, and histological evidence of fibroproliferative pulmonary processes in patients with COVID-19 ARDS.

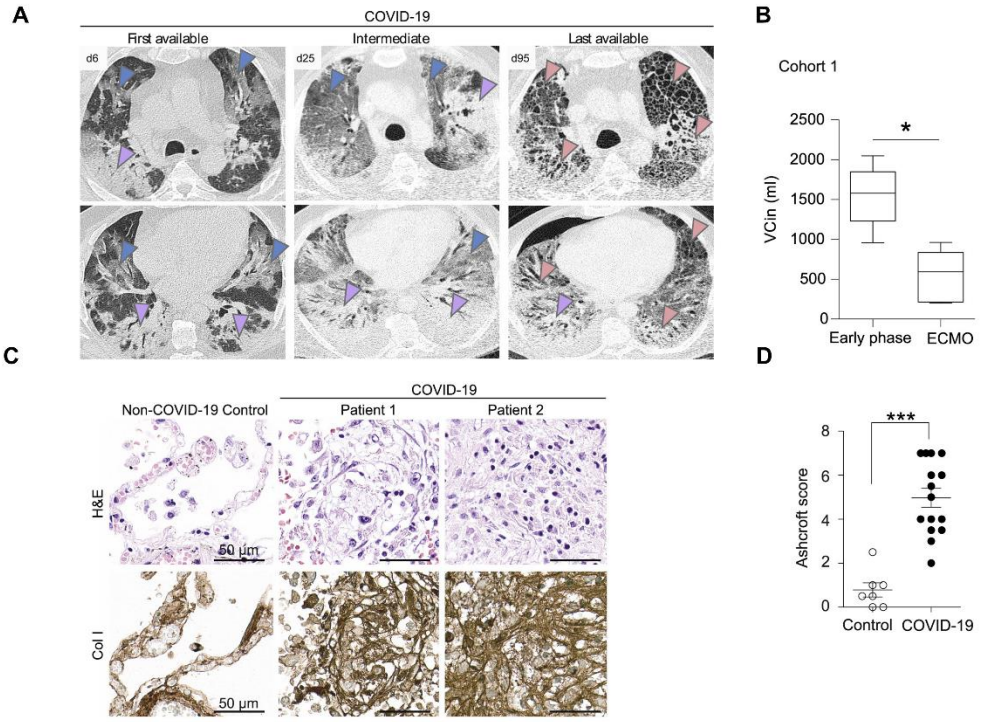

Figure 6: Evidence of fibrotic remodeling in pulmonary tissues in severe COVID-19.

(A) Exemplary CT scans of a COVID-19 ARDS patient with progressing fibrosis during hospitalization despite lung protective ventilation. Apical and basal lung crosssections are shown in the upper and lower row, respectively. Days post-symptom onset are indicated in the upper left corners. [adapted from Wendisch,... et al., 2021 **(B)** Inspiratory vital capacity of 16 COVID-19 ARDS patients at initiation of veno-venous ECMO and trough values during ECMO. [adapted from Wendisch,... et al., 2021 **(C.)** Exemplary H&E and Collagen I stained pulmonary tissue sections of fibrotic areas in COVID-19. [adapted from Wendisch,... et al., 2021 **(D)** Ashcroft scores, indicating fibrotic histological features, in 14 autopsy samples and one biopsy from 15 patients with COVID-19 ARDS and seven non-COVID-19 controls from five non-COVID-19 autopsies and 2 biopsies. The mean value of 2 independent assessments by experienced pathologists. [adapted from Wendisch,... et al., 2021

3.2.4 Gene set similarity of lung macrophages in COVID-19 ARDS and pulmonary fibrosis

Due to clinical observation of fibrosis and prominent expression of genes implicated in tissue remodeling in BAL macrophages, we aimed to assess the transcriptional similarity of pulmonary macrophages in COVID-19 to macrophages found in fibrotic lung disease. We therefore collected genesets of three published scRNA-seq studies of pulmonary fibrosis and controls (**Table 1**). In these studies, three gene sets were most specific for clusters of macrophages found in pulmonary fibrosis. In contrast, one geneset consisted of differentially expressed genes between fibrosis and controls across all macrophages and represents an average of different macrophage states. The fibrosis-associated gene sets from the three independent studies had 5 genes in common (LGMN, SDC2, CD84, GPNMB, and SPP1) and a pairwise intersection of 2 (LILRB4 and CTZ), 2 (APOE and MMP9), and 4 genes (CCL2, CHIT1, CD14, and FNIP2) (**Fig. 7A**).

We computed module scores per cell, which approximate average logarithmic fold changes of the tested gene sets in comparison to a control group of genes randomly chosen from bins with similar average expression as the tested gene set. According to our hypothesis, gene sets of fibrosis-expanded macrophages were significantly and specifically enriched in the LGMN/CD163-Mφ cluster **(Fig. 7B/C**). Interestingly, the effect sizes from all shared genes of the published data sets were even larger (**Fig. 7C/B**). Interestingly, LGMN and SPP1, but not CD163, contributed strongly to an increase in effect sizes of module score enrichment (**Fig. 7B/C**).

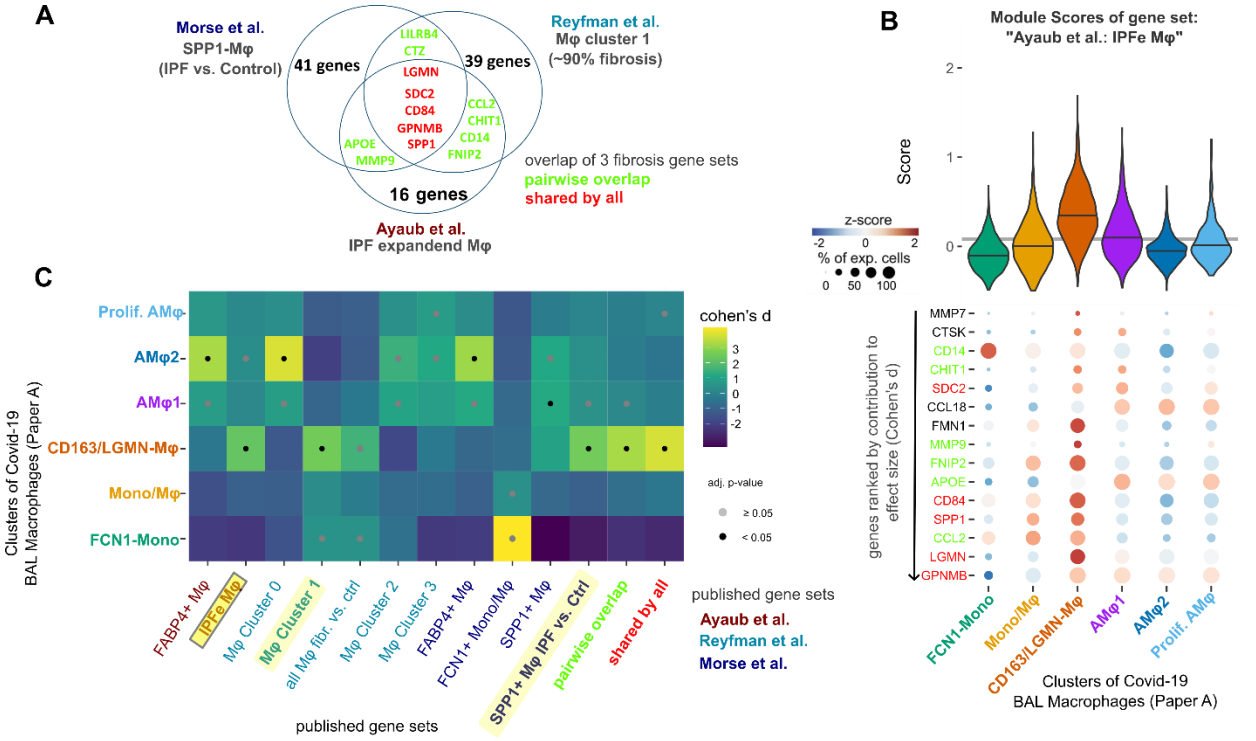

Figure 7: Genes characteristic of fibrosis-associated macrophages are enriched in LGMN/CD163 BAL macrophage.

(A) Venn diagram of gene sets of clusters most specific for fibrosis-associated macrophages from three published scRNA-seq studies of pulmonary fibrosis. [own figure with data from Wendisch... et al., 2021] **(B) Top**: Violin plot of cell-wise module scores of gene set of IPF-expanded macrophages from Ayaub et al. 2021 in BAL clusters of publication A. **Bottom**: Dotplot of the 15 genes with the strongest positive influence on effect size (Cohen's d) of the comparison: module score in LGMN/CD163-Mφ versus cells from all other clusters. Genes are ranked by reduction of module score effect size when the particular gene is left out. The dot color reflects the z-score of average gene expression in clusters according to the color scale. Module score effect sizes are calculated with each donor cluster as a data point. Gene names are colored as in (A). [own figure and figure modified with data from Wendisch,... et al., 2021] **(C)** Heat map of effect sizes of the comparison of gene set module scores of each BAL cluster on the y-axis versus all other BAL clusters measured by Cohen's d. Grey dots indicate Benjamini-Hochberg adjusted p-values <0.05 in the T-test of all top 2 effect sizes in each geneset. Gene sets as described in Table 1, and gene set names are colored-coded according to original publication. Genesets from (A) are highlighted in yellow. The gene set of name (B) "IPF expanded Macrophages" is marked with an additional grey box. [own figure with data from Wendisch,... et al., 2021]

Table 1: Published scRNA-seq gene sets of pulmonary fibrosis lung macrophages.

Dataset reference	Dataset description	Geneset name	Cluster description
Reyfman et al. (2019)[75]	8 healthy lung transplant donors,eight recipients with pulmonary fibrosis and one IPF cryo biopsy. Fibrosis = 4 IPF, 1HP, 2 SSC-ILD, 1 PM-ILD, 1 cryo biopsy IPF, no difference in clustering of different causes of fibrosis.	Mφ Cluster 0	~50 % cells of fibrosis donors.
		Mφ Cluster 1	**~90 % fibrosis cells of fibrosis donors**
		Mφ cluster 2	100% fibrosis donors, just 5 of the top 10 genes are immunoglobulin related, likely clustering due to contamination
		Mφ cluster 3	~40% cells of fibrosis donors, small cluster
		Fibrosis gene set	Not cluster specific, DE genes fibrosis/donor over all macrophages, no adjustment for donor or sample cell number, top 50 DE genes by lfold change
Morse et al. (2019)[55]	3 healthy lung explant donors, lower and upper lobe samples of 3 IPF patients. Lower lobes showed markedly more extensive fibrosis. Statistical procedure: Bonferroni adjusted pseudo-p-values from Wilcoxon ranked sum test cell-wise comparisons without blocking.	FAP4·Mφ	Mostly control and upper lobe IPF
		SPP1·Mφ	Approximately equal numbers of ctrl, upper, and lower lobe IPF
		SPP1·IPF	**Differentially expressed genes in SPP1 subset IPF vs. ctrl**
		FCN1·Mono/Mφ	Controle > upper lobe IPF > lower lobe IPF
Ayaub et al.[76]	Data from Adams et al. scRNA-seq of explanted lungs; 32 IPF, 28 smoker and nonsmoker controls, and 18 chronic obstructive pulmonary disease (COPD) lungs. Statistical procedure: DE genes versus two other macrophage groups. Differential gene testing of average gene expressions over donors and cell group using MAST[77]. Three macrophage groups were delineated by PHATE embedding[78]	**IPF expanded Mφ**	**Differentially expressed genes IPF expanded macrophages vs. monocytes and FABP4+ macrophages.**

Fibrosis-associated macrophage gene sets are marked with bold font. [original table summarizing the gene sets in the indicated publications] (Mφ: Macrophage)

3.2.5 Transcriptome proximity analysis of lung macrophages in COVID-19 and pulmonary fibrosis

To verify the validity of our results, we next integrated our BAL macrophage transcriptome in a joint embedding with other scRNA-seq data of lung macrophages in COVID-19 and pulmonary fibrosis using the scVI method (**Fig. 8A**). This data was obtained from one study of whole explanted fibrotic lungs after Covid-19 and two further studies of pulmonary fibrosis, mainly idiopathic pulmonary fibrosis, that included controls of donors with non-diseased lung tissue[53–55]. Interestingly, LGMN expression was enriched in locations of the integrated gene space of high density of macrophages from pulmonary fibrosis (**Fig. 8B/C**). Cells of the LGMN/CD163-Mφ cluster and a macrophage cluster from another COVID-19 study (Bharat et al.; MoM3) were mainly embedded in this area (**Fig. 8D**).

We devised a proximity score in which a reference cell was counted as related to a cell subset if the majority of its k-nearest neighbors in the integrated gene space belonged to the respective subset. Confirming our previous results, a significant fraction of LGMN/CD163-Mφ, as well as MoM3, were of high proximity to macrophages of pulmonary fibrosis datasets compared to control cells (**Fig. 8E/F**). Next to proliferating AM, no other cell cluster showed evidence for non-random proximity to fibrosis macrophages (**Fig. 8E/F**). All in all, next to the enrichment of published fibrosis-associated macrophage gene set, transcriptome integration of fibrosis and COVID-19 scRNA-seq data unveiled transcriptional similarity of LGMN/CD163-Mφ of COVID-19 BALs to lung macrophages found in pulmonary fibrosis.

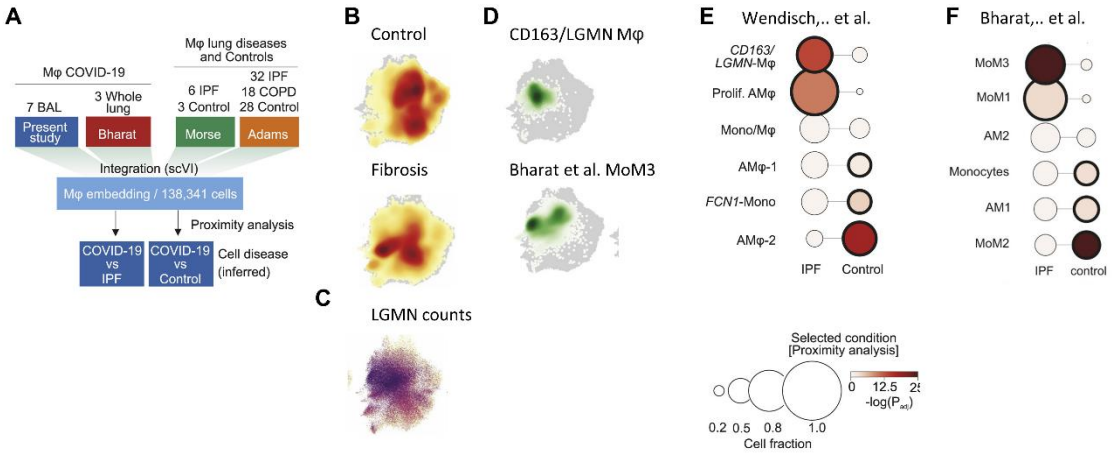

Figure 8: Proximity of transcriptomes of Covid-19 BAL LGMN/CD163-macrophages and lung macrophages from donors with pulmonary fibrosis.

(A) Diagram of integration strategy of our BAL macrophage dataset, a second COVID-19 macrophage dataset, and two large pulmonary fibrosis datasets. [adapted from Wendisch,... et al., 2021] **(B)** Density of cells of control and pulmonary fibrosis datasets as in (A) in the scVI-integrated gene space. [adapted from Wendisch,... et al., 2021] **(C)** LGMN counts of cells of the integrated gene space of (B). [adapted from Wendisch,... et al. 2021] **(D)** Density cells of LGMN/CD163-Mφ from our BAL dataset and the similar cluster from Bharat et al., 2021 as in (A) in the scVI integrated gene space. [adapted from Wendisch,... et al. 2021] **(E)** Proximity analysis of BAL macrophages grouped into separate clusters to macrophages from publications of fibrotic lung disease (mainly IPF) or controls of unaffected lung tissue. [adapted from Wendisch,... et al. 2021] **(F)** As in (E) with macrophage data of Bharat et al., 2020[54]. [adapted from Wendisch,... et al. 2021]

3.2.6 SARS-CoV-2 stimulation of human primary monocytes in vitro induces a profibrotic gene program.

Next, we asked if the interaction of SARS-CoV-2 and macrophages might directly trigger the observed fibrosis-associated signatures. To this end, we conducted a scRNA-seq in-vitro stimulation experiment with human, primary FACS-sorted $CD14^{+}CD16^{lo}$ Monocytes. Monocytes were stimulated with high titers of authentic SARS-CoV-2 virus for 18 hours. As controls, we added the RIG-I agonist 5' triphosphate hairpin RNA (3p-hpRNA) and the Toll-like receptor (TLR)-7/-8 agonist R848, which activate prototypical pathways of antiviral and inflammatory responses (**Fig. 9A**). All conditions were separable in UMAP embeddings; however, SARS-CoV-2 showed partial overlap with 3p-hpRNA stimulation that resulted in type-I interferon (IFN) inducible gene signatures (**Fig. 9B/D**).

Transcription factor target over-representation analysis predicted the same top TF genes for SARS-CoV-2 stimulated genes as were predicted for DE genes in LGMN/CD163-Mφ of the BAL of COVID-19 ARDS patients (**Fig. 9C/5C**). Interestingly, multiple genes that were found significantly upregulated in lung macrophages of COVID-19 and pulmonary fibrosis, such as CD163, MERTK, and LGMN were differentially acti-

vated upon exposure to SARS-CoV-2 (**Fig. 9D**). In contrast to R848, SARS-CoV-2 stimulation induced only limited or no expression of inflammatory hallmarks such as interleukin 1-beta (IL1B) and interleukin 6 (IL6) (**Fig. 9D**).

This prompted us to test if SARS-CoV-2 may directly induce the previously found fibrosis-associated signatures in lung LGMN/CD163-Mφs of COVID-19 patients. Indeed, module scores of published fibrosis-associated macrophage gene sets were enriched in SARS-CoV-2 stimulated monocytes compared to the other conditions (**Fig. 9E**, paper A Fig. 6E).

For orthogonal validation at the protein level, we stimulated human $CD14^{+}CD16^{lo}$ monocytes with SARS-CoV-2 or Influenza A virus (IAV) for 3, 5, or 18 hours and measured sequence-specific protein abundance with quantitative mass spectroscopic proteomics (**Fig. 9A**). In 2 replicates from 4 donors we quantified 6,951 proteins and 5,299 phosphorylation sites. SARS-CoV-2 and IAV induced divergent changes in the macrophage proteome, particularly at 18 hours post-infection **(Fig. 7C)**. Similar to the scRNA-seq data, fibrosis-associated macrophage signatures were highly enriched in monocytes stimulated with SARS-CoV-2 for 18 hours. Interestingly, this was not detected in IAV-infected cells (**Fig. 9F**). Notably, gene set enrichment analysis of protein intensity ratios of SARS-CoV-2 over IAV infection showed highly significant enrichment for extracellular matrix assembly **(Fig. 9G)**.

Lastly, we evaluated whether the observed responses of monocytes to SARS-COV-2 stimulation could result from a productive infection. Over 18 hours, IAV-infected monocytes showed a significant production of IAV proteins. However, SARS-COV-2 stimulated monocytes showed no significant viral protein accumulation (**Fig. 9H**).

We concluded that SARS-CoV-2, but not IAV, directly triggers monocyte polarization towards fibrosis-associated signatures, excluding productive infection as a cause.

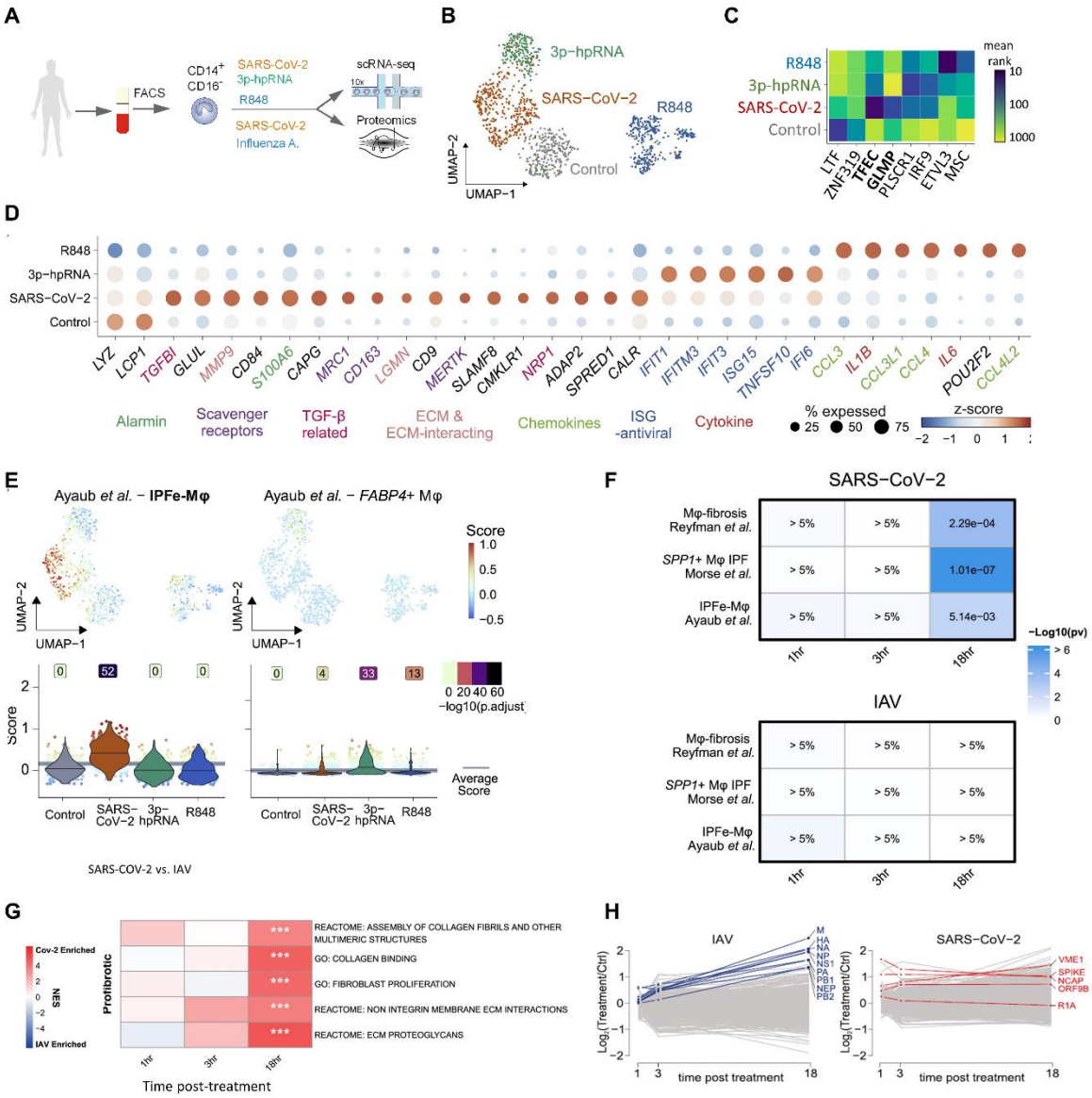

Figure 9: SARS-CoV-2 directly constitutes a trigger for monocytes to express fibrosis-associated gene signatures.

(A) Graphical representation of the experimental setup of *in-vitro* stimulation of primary human monocytes and read out via scRNA-seq and mass spectrometry. [adapted from Wendisch,... et al., 2021] **(B)** UMAP of scRNA-seq data of sorted human peripheral blood monocytes after 18 hours of stimulation with SARS-COV-2, 5'-triphosphate-hairpin RNA, a RIG-I agonist, and the Toll-like receptor agonist R848. [adapted from Wendisch,... et al., 2021] **(C)** Top two predicted transcription factors per condition. GLMP and TFEC were likewise the most highly predicted transcription factors in BAL CD163/LGMN macrophages. Transcription factor target over-representation analysis based on differentially expressed genes of the clusters. The color gradient displays the mean rank of ChIP-X Enrichment Analysis 3 (CHEA3)74-prediction based on Chip-Seq data. Rank 1 refers to the highest prediction score. [modified from Wendisch,... et al., 2021] **(D)** Dot plot of differentially expressed genes in scRNA-seq in each stimulated condition depicted in B. Gene categories or functions are color-coded.[adapted from Wendisch,... et al., 2021] **(E)** Module scores of gene signatures of IPF-expanded macrophages from Ayaub et al. 2021. UMAP embedding as in (B). Violin plots and cell-level Wilcoxon rank sum test derived p values.[adapted from Wendisch,... et al., 2021] **(F)** Heatmap representation of mass spectrometric protein quantification of the genes in the genesets indicated on the y-axis. P-values from a one-sided Wilcoxon signed-rank test indicating gene signature enrichment in a cumulative distribution function [adapted from Wendisch,... et al., 2021] **(G)** Gene set enrichment analysis of fibrosis-related gene ontology (GO) and Reactome terms. Comparing SARS-CoV-2 versus Influenza A virus stimulated monocyte protein quantification via mass spectrometry. (NES=normalized enrichment score). [adapted from Wendisch,... et al., 2021] **(H)** Log_2 fold changes of protein abundance of Influenza A and SARS-CoV-2 viral proteins (blue, red) in the respective conditions versus unstimulated controls. Host proteins are plotted in gray. [adapted from Wendisch,... et al., 2021]

4 Discussion

4.1 Brief Summary

This dissertation encompasses two dual-cohort studies identifying disease severity-specific macrophage and monocyte responses to early SARS-CoV-2 lineages assessed with diverse multiparametric methods[6,56].

In Paper B, we found disparate peripheral blood monocyte activation statuses in mild and severe COVID-19. Among the genes expressed at lower levels in severe COVID-19 monocytes were genes related to inflammatory antigen presentation, namely MHC II transcripts (HLA-DRA/DRB) and the costimulatory molecule CD83, as well as genes central to inflammatory processes (IL1B, IRF1) and antiviral responses (IFI44L, IFI27).

In paper A, we investigated macrophage responses to severe COVID-19 in affected lung tissues and expanded our findings with *in vitro* monocyte stimulation. Remarkably, we found macrophage the gene signatures associated with fibrotic pulmonary disease, such as IPF, in BAL-macrophages also in monocytes stimulated *in vitro* with SARS-COV-2. Furthermore, we provide evidence of fibroproliferative disease courses in severe COVID-19.

4.2 Interpretation of results

4.2.1 Publication B

Here, we report decreased expression of core effector molecules of antigen-presentation and inflammatory co-signaling such as HLA-DR, CD83, and IL-1β in peripheral monocytes of severe COVID-19 compared to mild cases. (**Fig. 2E/F/G**). MHC II molecules such as HLA-DR present antigens to T cells, thereby initiating an adaptive immune response[79]. A low expression may, therefore, compromise the ability of the immune system to recognize and respond to pathogens[80].

HLA-DR^{lo} monocytes have previously been associated with adverse outcomes in infectious diseases and immunosuppression in sepsis[81–83]. CD83 is a co-stimulatory molecule to MHC II binding for ensuing T-cell activation[79]. Signaling through CD83 binding initiates both regulatory and inflammatory T-cell responses; therefore, the results of the

relative absence of CD83 may be diverse[84]. Nevertheless, CD83 expression is in line with increased antigen-presentation.

IL-1β is a pro-inflammatory cytokine. Low expression of IL-1β in monocytes may result in reduced inflammatory responses, potentially impairing the ability of the immune system to mount effective defense mechanisms dependent on NF-κB regulated genes[85]. Nonetheless, immune responses have to be balanced for effect and harm to secure adequate function of the organism[73]. Therefore, the lower levels of inflammatory mediators detected in COVID-19 monocytes may also reflect physiological processes aiming at the tolerability of the yet ongoing immune response[86].

Monocytes in severe COVID-19 concurrently expressed higher levels of calgranulins (S100A8/9/12) (**Fig. 2E/F/G**). High calgranulin levels are reported in sepsis and are involved in proinflammatory processes[87]. Calgranulins can be secreted in large amounts and are sensed as danger-associated molecular patterns (DAMP). They have antibacterial capacity through iron and manganese sequestration, and they have been implicated in prolonged post-infectious inflammation, serving, for example, as a biomarker for active inflammatory bowel disease[81,88,89]. Here, we identified concomitant low HLA-DR expression with high levels of S100A8/9/12, which may suggest a need to particularize the phenotyping of supposedly immunoparalysis-promoting monocytes in critical disease[81,83]. Dysfunctional innate antiviral activity in severe COVID-19 may be at play considering the lower expression of mediators of innate antiviral response like the transcription factors IRF1 and interferon response genes like IFI44L and IFI27(**Fig. 2G**)[90].

Initially intriguing were high levels of CD163 in peripheral monocytes of both mild and severe COVID-19 (**Fig. 2G/H**). The heme-haptoglobin complex scavenger receptor CD163 has been brought into relation with tissue repair properties of macrophages, associated with fibrosis and so-called “alternative” activation[91–95]. While removing toxic, free hem prevents oxidative tissue damage, no direct mechanisms of CD163 being central to active tissue reconstitution are evident[3]. While macrophage CD163-expression correlates with restorative and profibrotic conditions, its expression may be independently regulated by heme through local bleeding and erythrocytolysis[93,94,96]. This aligns with its induction by diverse signals such as the proinflammatory IL-6 and IFN-γ and inflammation-suppressing glucocorticoids, likely reflecting a complex sensory circuitry[96].

4.2.2 Publication A

Intriguingly, CD163 expression was also increased in macrophages in pulmonary tissue of COVID-19 autopsy samples in the main study of this dissertation **(Fig. 4C/D/F).** ScRNA-seq of BAL macrophages allowed us further to assess pulmonary macrophages without the preselection of markers. Overall, macrophage clusters were not segregated, indicating gradual and overlapping differences in macrophage polarization (**Fig. 5A**). This aligns with a multidimensional and overlapping view of macrophage functions as opposed to the overcome dichotomous M1/M2 model[3,42,50].

We could identify three poles of significant differentiation. Namely FCN1$^+$ monocytic cells, FABP4$^+$ conventional alveolar macrophage, and LGMN/CD163-Mφ cluster (**Fig. 5A**). LGMN, an asparaginyl endopeptidase, was highly differentially expressed in this last cluster (**Fig. 5D**). Amongst its many substrates, LGMN can activate Matrix-Metallo-Proteases (MMP) 2 & 9, which in turn can activate TGF-β and VEGF, which act as key inducers of tissue proliferation and regeneration[97,98]. Although LGMN has been associated with profibrotic function, it has also been ascribed to fibrosis resolution[72,99]. Furthermore, LGMN has been associated with both hypothetic macrophage types in different settings[72,100], highlighting another example of the reduced utility of the M1/ M2 concept.

Among transcripts enriched in LGMN/CD163-Mφ was osteopontin (SPP1), a matricellular protein and ligand to class alpha integrins implied in tissue remodeling processes (Fig. 5D). SPP1+ macrophages have previously been associated with pulmonary fibrosis and named profibrotic macrophages[55,101,102]. However, in the light of the vast amount of functions attributed to osteopontin and the fact that SPP1 knock-out does not result in a cessation of fibrosis but rather histological alteration, the causality implied by the syllable “pro-” (Greek/Latin: “before”) may be an overstatement in relation to SPP1 expression alone[103,104]. Nevertheless, LGMN and SPP1 were among a core signature of 5 genes of fibrosis-associated macrophages in 3 publications on pulmonary fibrosis **(Table 1)**. By utilizing different computational methods, we show that BAL-macrophages in the early phase of COVID-19 ARDS share this fibrosis-associated gene signature (**Fig. 6/7/8**). Unlike LGMN and SPP1, here we show that despite its concomitant upregulation in COVID-19 and pulmonary fibrosis, CD163 is not strongly discriminatory for a fibrosis-associated macrophage phenotype **(Figure 7A/B)**. This highlights modern “omics” technologies' strength by not having to rely on marker genes for classification.

Furthermore, we demonstrated that *in-vitro* exposure of primary human monocytes to SARS-CoV-2, but not IAV, also induces these fibrosis-associated gene signatures (**Fig. 9D-F**). Predicted transcription factor activity in COVID-19 BAL LGMN/CD163-Mφ and in *in-vitro* SARS-CoV-2 stimulated monocytes was identical for the top two results (TFEC and GLMP) (**Fig. 5C/9C**). However, this prediction's in-vivo accuracy remains to be shown in future experiments. Although in vivo alternative causes could be present, SARS-CoV-2 may, therefore, directly influence *in-vivo* macrophage states. In line with this, long-lasting profibrotic pathology triggered by strong initial impulses has been previously described[105].

LGMN/CD163-Mφ as well as SARS-CoV-2 stimulated monocytes were enriched for NRP1, a co-receptor for multiple growth factors, such as TGF-β and VEGF-A and also involved in (fibro-)proliferative processes(Fig. 5C, 9D)[106,107]. Notably, NRP1 is also a co-receptor for SARS-CoV-2 through the bindings of the 3‘ end of S1, which is freed by cleavage of the S-Protein at the furin cleavage site (FCS)[108,109]. While we did not find evidence for productive infection, this could be a potential mechanism of interaction between macrophages and SARS-CoV-2 (Fig. 9H). The in vitro experiments reported here were conducted with early SARS-CoV-2 isolates without mutations at the FCS. However, the PRRAR amino acid motif that binds to NRP1 is mutated in all variants of concern (e.g. P681H), which is predicted to result in lower affinity to NRP1[109]. To assess this hypothesized mechanism of interaction, future studies could compare the effects of furin cleavage site mutants on NRP1-expressing macrophages, with a possible cessation of the fibrosis-associated macrophage polarization reported here.

4.3 Strengths and weaknesses

Both underlying studies consisted of dual cohorts of patients suffering from COVID-19. Due to the unforeseen onset of the COVID-19 pandemic, the studies were initiated with a hypothesis-generating intent with a subcohort of the PA-COVID-19 study, a prospective observational cohort study at the Berlin University Hospital Charité. Inclusion in this study resulted from a combination of biomaterial availability, ethical soundness of the procedures in individual cases, and patient consent. The findings were validated in separated cohorts. Therefore, although decisive care was taken to minimize investigator biases, these cannot be excluded to the extent of a fully blinded study with preset endpoints.

Furthermore, scRNA-seq is a relatively young field in which even basic analytical methods are still evolving and have not reached widespread consensus. For example, even the most fundamental methods, such as differential gene expression testing, are still being improved, and suggested methods are not sufficiently benchmarked[110]. Here, the most prominent changes are reported, which are unlikely to be affected by method selection. All “omic”-data is made available online, allowing future discovery with newly developed techniques.

While we demonstrate the direct effects of SARS-CoV-2 on the induction of macrophage programs *in vitro*, direct *in-vivo* virus-macrophage interactions are challenging to determine in human studies. Furthermore, the molecular mechanisms underlying the induction of fibrosis-associated genes by SARS-CoV-2 and the causes of the different activation profile observed in monocytes in severe and mild COVID-19 remain to be elucidated in greater detail.

Due to the nonlinear nature of complex tissue processes like pulmonary fibrosis, sophisticated modeling approaches of reciprocal cell interactions might pose the only satisfactory approach towards predicting the outcome of tissue perturbations[105]. Through the multidimensionality of the data presented in this dissertation, this work may form an informative basis for complex modeling of such kind.

4.4 Conclusion

Dysregulated immune responses aggravate COVID-19[19,111–113]. To identify predictive biomarkers and therapeutic targets, detailed knowledge of the cellular processes differing in mild and potentially fatal courses of COVID-19 is urgently needed. Macrophages are key immune sentinels and orchestrators of pulmonary tissue homeostasis. To gain an understanding of the host factors of the newly emerged viral disease, the work underlying this dissertation investigated disease severity-related responses of macrophages and monocytes to SARS-CoV-2.

We demonstrated reduced levels of markers of antigen-presentation, inflammation, and antiviral responses in monocytes of severe compared to mild COVID-19.
Furthermore, we revealed the similarity of COVID-19 BAL LGMN/CD163-Mφ to macrophages in pulmonary fibrotic disease, such as IPF, with two complementary techniques. Enrichment of fibrosis-associated signatures in macrophages was consistent over three

datasets and also found in a second COVID-19 BAL study, with shared genes being more abundant than the individual gene sets. To our knowledge, this was the first study to report on the commonality of pulmonary macrophage transcripts in pulmonary fibrosis and viral ARDS.

It will be important to dissect the molecular mechanisms linking fibrosis-associated macrophage polarization and fibrosis and the causes for the observed signature in severe COVID-19, as these may provide new targets for therapeutic intervention.

References

1. Sikkema, L. et al. An integrated cell atlas of the lung in health and disease. Nat. Med. 29, 1563–1577 (2023).
2. Gordon, S. Elie Metchnikoff: father of natural immunity. Eur. J. Immunol. 38, 3257–3264 (2008).
3. Okabe, Y. & Medzhitov, R. Tissue biology perspective on macrophages. Nat. Immunol. 17, 9–17 (2015).
4. Park, M. D., Silvin, A., Ginhoux, F. & Merad, M. Macrophages in health and disease. Cell 185, 4259–4279 (2022).
5. van Furth, R. et al. The mononuclear phagocyte system: a new classification of macrophages, monocytes, and their precursor cells. Bull. World Health Organ. 46, 845–852 (1972).
6. Schulte-Schrepping, J. et al. Severe COVID-19 Is Marked by a Dysregulated Myeloid Cell Compartment. Cell 182, 1419–1440.e23 (2020).
7. Richardson, S. et al. Presenting Characteristics, Comorbidities, and Outcomes Among 5700 Patients Hospitalized With COVID-19 in the New York City Area. JAMA 323, 2052–2059 (2020).
8. Osuchowski, M. F. et al. The COVID-19 puzzle: deciphering pathophysiology and phenotypes of a new disease entity. Lancet Respir Med 9, 622–642 (2021).
9. Gujski, M., Jankowski, M., Rabczenko, D., Goryński, P. & Juszczyk, G. The Prevalence of Acute Respiratory Distress Syndrome (ARDS) and Outcomes in Hospitalized Patients with COVID-19-A Study Based on Data from the Polish National Hospital Register. Viruses 14, (2022).
10. CDC COVID-19 Response Team. Severe Outcomes Among Patients with Coronavirus Disease 2019 (COVID-19) - United States, February 12-March 16, 2020. MMWR Morb. Mortal. Wkly. Rep. 69, 343–346 (2020).
11. Ferguson, N. D. et al. The Berlin definition of ARDS: an expanded rationale, justification, and supplementary material. Intensive Care Med. 38, 1573–1582 (2012).
12. Wilkinson, E. RECOVERY trial: the UK covid-19 study resetting expectations for clinical trials. BMJ 369, m1626 (2020).
13. RECOVERY Collaborative Group et al. Dexamethasone in Hospitalized Patients with Covid-19. N. Engl. J. Med. 384, 693–704 (2021).
14. Abani, O. et al. Tocilizumab in patients admitted to hospital with COVID-19 (RECOVERY): a randomised, controlled, open-label, platform trial. Lancet 397, 1637–1645 (2021).
15. Marconi, V. C. et al. Efficacy and safety of baricitinib for the treatment of hospitalised adults with COVID-19 (COV-BARRIER): a randomised, double-blind, parallel-group, placebo-controlled phase 3 trial. Lancet Respir Med 9, 1407–1418 (2021).
16. RECOVERY Collaborative Group. Baricitinib in patients admitted to hospital with COVID-19 (RECOVERY): a randomised, controlled, open-label, platform trial and updated meta-analysis. Lancet 400, 359–368 (2022).
17. Zayed, Y. et al. Use of glucocorticoids in patients with acute respiratory distress syndrome: a meta-analysis and trial sequential analysis. J. Intensive Care Med. 8, 43 (2020).
18. Villar, J. et al. Dexamethasone treatment for the acute respiratory distress syndrome: a multicentre, randomised controlled trial. Lancet Respir Med 8, 267–276 (2020).
19. Zhou, P. et al. A pneumonia outbreak associated with a new coronavirus of probable bat origin. Nature 579, 270–273 (2020).
20. Braun, J. et al. SARS-CoV-2-reactive T cells in healthy donors and patients with COVID-19. Nature 587, 270–274 (2020).
21. Grobben, M. et al. Cross-reactive antibodies after SARS-CoV-2 infection and vaccination. Elife 10, (2021).
22. Pifarré I Arolas, H. et al. Years of life lost to COVID-19 in 81 countries. Sci. Rep. 11, 3504 (2021).
23. Byrne, A. J., Mathie, S. A., Gregory, L. G. & Lloyd, C. M. Pulmonary macrophages: key players in the innate defence of the airways. Thorax 70, 1189–1196 (2015).
24. Yu, X. et al. The Cytokine TGF-β Promotes the Development and Homeostasis of Alveolar Macrophages. Immunity 47, 903–912.e4 (2017).
25. McKee, C. M. et al. Hyaluronan (HA) fragments induce chemokine gene expression in alveolar macrophages. The role of HA size and CD44. J. Clin. Invest. 98, 2403–2413 (1996).
26. Burke, B. et al. Expression of HIF-1alpha by human macrophages: implications for the use of macrophages in hypoxia-regulated cancer gene therapy. J. Pathol. 196, 204–212 (2002).
27. White, J. R. et al. Genetic amplification of the transcriptional response to hypoxia as a novel means of identifying regulators of angiogenesis. Genomics 83, 1–8 (2004).
28. Stanley, E. et al. Granulocyte/macrophage colony-stimulating factor-deficient mice show no major perturbation of hematopoiesis but develop a characteristic pulmonary pathology. Proc. Natl. Acad. Sci. U. S. A. 91, 5592–5596 (1994).

29. Aegerter, H. et al. Influenza-induced monocyte-derived alveolar macrophages confer prolonged antibacterial protection. Nat. Immunol. 21, 145–157 (2020).
30. Satoh, T. et al. Identification of an atypical monocyte and committed progenitor involved in fibrosis. Nature 541, 96–101 (2016).
31. Sato, M., Muragaki, Y., Saika, S., Roberts, A. B. & Ooshima, A. Targeted disruption of TGF-beta1/Smad3 signaling protects against renal tubulointerstitial fibrosis induced by unilateral ureteral obstruction. J. Clin. Invest. 112, 1486–1494 (2003).
32. Koh, T. J. & DiPietro, L. A. Inflammation and wound healing: the role of the macrophage. Expert Rev. Mol. Med. 13, e23 (2011).
33. Gerhardt, T. & Ley, K. Monocyte trafficking across the vessel wall. Cardiovasc. Res. 107, 321–330 (2015).
34. Larsen, C. G., Zachariae, C. O., Oppenheim, J. J. & Matsushima, K. Production of monocyte chemotactic and activating factor (MCAF) by human dermal fibroblasts in response to interleukin 1 or tumor necrosis factor. Biochem. Biophys. Res. Commun. 160, 1403–1408 (1989).
35. Bardina, S. V. et al. Differential Roles of Chemokines CCL2 and CCL7 in Monocytosis and Leukocyte Migration during West Nile Virus Infection. J. Immunol. 195, 4306–4318 (2015).
36. Ginhoux, F. & Guilliams, M. Tissue-Resident Macrophage Ontogeny and Homeostasis. Immunity 44, 439–449 (2016).
37. Ng, L. G., Liu, Z., Kwok, I. & Ginhoux, F. Origin and Heterogeneity of Tissue Myeloid Cells: A Focus on GMP-Derived Monocytes and Neutrophils. Annu. Rev. Immunol. 41, 375–404 (2023).
38. Chavakis, T., Mitroulis, I. & Hajishengallis, G. Hematopoietic progenitor cells as integrative hubs for adaptation to and fine-tuning of inflammation. Nat. Immunol. 20, 802–811 (2019).
39. Pietras, E. M. et al. Chronic interleukin-1 exposure drives haematopoietic stem cells towards precocious myeloid differentiation at the expense of self-renewal. Nat. Cell Biol. 18, 607–618 (2016).
40. van Furth, R. Macrophage activity and clinical immunology. Origin and kinetics of mononuclear phagocytes. Ann. N. Y. Acad. Sci. 278, 161–175 (1976).
41. Daems, W. T. & de Bakker, J. M. Do resident macrophages proliferate? Immunobiology 161, 204–211 (1982).
42. Hashimoto, D. et al. Tissue-resident macrophages self-maintain locally throughout adult life with minimal contribution from circulating monocytes. Immunity 38, 792–804 (2013).
43. Ajami, B., Bennett, J. L., Krieger, C., Tetzlaff, W. & Rossi, F. M. V. Local self-renewal can sustain CNS microglia maintenance and function throughout adult life. Nat. Neurosci. 10, 1538–1543 (2007).
44. Kuziel, W. A. et al. Severe reduction in leukocyte adhesion and monocyte extravasation in mice deficient in CC chemokine receptor 2. Proc. Natl. Acad. Sci. U. S. A. 94, 12053–12058 (1997).
45. Mills, C. D., Kincaid, K., Alt, J. M., Heilman, M. J. & Hill, A. M. M-1/M-2 macrophages and the Th1/Th2 paradigm. J. Immunol. 164, 6166–6173 (2000).
46. Xue, J. et al. Transcriptome-based network analysis reveals a spectrum model of human macrophage activation. Immunity 40, 274–288 (2014).
47. Guilliams, M. & van de Laar, L. A Hitchhiker's Guide to Myeloid Cell Subsets: Practical Implementation of a Novel Mononuclear Phagocyte Classification System. Front. Immunol. 6, 406 (2015).
48. Adler, M., Chavan, A. R. & Medzhitov, R. Tissue Biology: In Search of a New Paradigm. Annu. Rev. Cell Dev. Biol. 39, 67–89 (2023).
49. Sanin, D. E. et al. A common framework of monocyte-derived macrophage activation. Sci Immunol 7, eabl7482 (2022).
50. Bian, Z. et al. Deciphering human macrophage development at single-cell resolution. Nature 582, 571–576 (2020).
51. Korsunsky, I. et al. Fast, sensitive and accurate integration of single-cell data with Harmony. Nat. Methods 16, 1289–1296 (2019).
52. Reyes, M. et al. An immune-cell signature of bacterial sepsis. Nat. Med. 26, 333–340 (2020).
53. Adams, T. S. et al. Single-cell RNA-seq reveals ectopic and aberrant lung-resident cell populations in idiopathic pulmonary fibrosis. Science Advances 6, eaba1983 (2020).
54. Bharat, A. et al. Lung transplantation for patients with severe COVID-19. Sci. Transl. Med. 12, (2020).
55. Morse, C. et al. Proliferating SPP1/MERTK-expressing macrophages in idiopathic pulmonary fibrosis. Eur. Respir. J. 54, (2019).
56. Wendisch, D. et al. SARS-CoV-2 infection triggers profibrotic macrophage responses and lung fibrosis. Cell 184, 6243–6261.e27 (2021).

57. Pascual-Reguant, A. et al. Multiplexed histology analyses for the phenotypic and spatial characterization of human innate lymphoid cells. Nat. Commun. 12, 1737 (2021).
58. Holzwarth, K. et al. Multiplexed fluorescence microscopy reveals heterogeneity among stromal cells in mouse bone marrow sections. Cytometry A 93, 876–888 (2018).
59. Schubert, W. et al. Analyzing proteome topology and function by automated multidimensional fluorescence microscopy. Nat. Biotechnol. 24, 1270–1278 (2006).
60. Schindelin, J. et al. Fiji: an open-source platform for biological-image analysis. Nat. Methods 9, 676–682 (2012).
61. McInnes, L., Healy, J. & Melville, J. UMAP: Uniform Manifold Approximation and Projection for Dimension Reduction. arXiv [stat.ML] (2018).
62. Hao, Y. et al. Integrated analysis of multimodal single-cell data. Cell 184, 3573–3587.e29 (2021).
63. Haghverdi, L., Lun, A. T. L., Morgan, M. D. & Marioni, J. C. Batch effects in single-cell RNA-sequencing data are corrected by matching mutual nearest neighbors. Nat. Biotechnol. 36, 421–427 (2018).
64. Wolf, F. A., Angerer, P. & Theis, F. J. SCANPY: large-scale single-cell gene expression data analysis. Genome Biol. 19, 15 (2018).
65. Heaton, H. et al. Souporcell: robust clustering of single-cell RNA-seq data by genotype without reference genotypes. Nat. Methods 17, 615–620 (2020).
66. Mertins, P. et al. Reproducible workflow for multiplexed deep-scale proteome and phosphoproteome analysis of tumor tissues by liquid chromatography-mass spectrometry. Nat. Protoc. 13, 1632–1661 (2018).
67. Tyanova, S., Temu, T. & Cox, J. The MaxQuant computational platform for mass spectrometry-based shotgun proteomics. Nat. Protoc. 11, 2301–2319 (2016).
68. Wöbke, T. K., von Knethen, A., Steinhilber, D. & Sorg, B. L. CD69 is a TGF-β/1α,25-dihydroxyvitamin D3 target gene in monocytes. PLoS One 8, e64635 (2013).
69. Travis, M. A. & Sheppard, D. TGF-β activation and function in immunity. Annu. Rev. Immunol. 32, 51–82 (2014).
70. Reymond, N. et al. DNAM-1 and PVR regulate monocyte migration through endothelial junctions. J. Exp. Med. 199, 1331–1341 (2004).
71. Jiang, R., Sun, T., Song, D. & Li, J. J. Statistics or biology: the zero-inflation controversy about scRNA-seq data. Genome Biol. 23, 31 (2022).
72. Wang, D. et al. Legumain, an asparaginyl endopeptidase, mediates the effect of M2 macrophages on attenuating renal interstitial fibrosis in obstructive nephropathy. Kidney Int. 94, 91–101 (2018).
73. Meizlish, M. L., Franklin, R. A., Zhou, X. & Medzhitov, R. Tissue Homeostasis and Inflammation. Annu. Rev. Immunol. 39, 557–581 (2021).
74. Keenan, A. B. et al. ChEA3: transcription factor enrichment analysis by orthogonal omics integration. Nucleic Acids Res. 47, W212–W224 (2019).
75. Reyfman, P. A. et al. Single-Cell Transcriptomic Analysis of Human Lung Provides Insights into the Pathobiology of Pulmonary Fibrosis. Am. J. Respir. Crit. Care Med. 199, 1517–1536 (2019).
76. Ayaub, E. A. et al. Single Cell RNA-seq and Mass Cytometry Reveals a Novel and a Targetable Population of Macrophages in Idiopathic Pulmonary Fibrosis. bioRxiv 2021.01.04.425268 (2021) doi:10.1101/2021.01.04.425268.
77. Finak, G. et al. MAST: a flexible statistical framework for assessing transcriptional changes and characterizing heterogeneity in single-cell RNA sequencing data. Genome Biol. 16, 278 (2015).
78. Moon, K. R. et al. Visualizing structure and transitions in high-dimensional biological data. Nat. Biotechnol. 37, 1482–1492 (2019).
79. Iwasaki, A. & Medzhitov, R. Control of adaptive immunity by the innate immune system. Nat. Immunol. 16, 343–353 (2015).
80. Huseby, E. S. & Teixeiro, E. The perception and response of T cells to a changing environment are based on the law of initial value. Sci. Signal. 15, eabj9842 (2022).
81. Monneret, G. et al. Persisting low monocyte human leukocyte antigen-DR expression predicts mortality in septic shock. Intensive Care Med. 32, 1175–1183 (2006).
82. Zhang, D. P. et al. A decrease of human leucocyte antigen-DR expression on monocytes in peripheral blood predicts stroke-associated infection in critically-ill patients with acute stroke. Eur. J. Neurol. 16, 498–505 (2009).
83. Hynninen, M. et al. Predictive value of monocyte histocompatibility leukocyte antigen-DR expression and plasma interleukin-4 and -10 levels in critically ill patients with sepsis. Shock 20, 1–4 (2003).
84. Grosche, L. et al. The CD83 Molecule - An Important Immune Checkpoint. Front. Immunol. 11, 721 (2020).

85. Weber, A., Wasiliew, P. & Kracht, M. Interleukin-1 (IL-1) pathway. Sci. Signal. 3, cm1 (2010).
86. Venet, F., Demaret, J., Gossez, M. & Monneret, G. Myeloid cells in sepsis-acquired immunodeficiency. Ann. N. Y. Acad. Sci. 1499, 3–17 (2021).
87. Dubois, C. et al. High plasma level of S100A8/S100A9 and S100A12 at admission indicates a higher risk of death in septic shock patients. Sci. Rep. 9, 15660 (2019).
88. Narumi, K. et al. Proinflammatory Proteins S100A8/S100A9 Activate NK Cells via Interaction with RAGE. J. Immunol. 194, 5539–5548 (2015).
89. Riva, M. et al. Induction of nuclear factor-κB responses by the S100A9 protein is Toll-like receptor-4-dependent. Immunology 137, 172–182 (2012).
90. McNab, F., Mayer-Barber, K., Sher, A., Wack, A. & O'Garra, A. Type I interferons in infectious disease. Nat. Rev. Immunol. 15, 87–103 (2015).
91. Kristiansen, M. et al. Identification of the haemoglobin scavenger receptor. Nature 409, 198–201 (2001).
92. Tremble, L. F., Forde, P. F. & Soden, D. M. Clinical evaluation of macrophages in cancer: role in treatment, modulation and challenges. Cancer Immunol. Immunother. 66, 1509–1527 (2017).
93. Nouno, T. et al. Elevation of pulmonary CD163+ and CD204+ macrophages is associated with the clinical course of idiopathic pulmonary fibrosis patients. J. Thorac. Dis. 11, 4005–4017 (2019).
94. Vasarmidi, E. et al. Evaluation of CD163 expression on alveolar macrophages from BAL of patients with Fibrotic Lung Diseases. Eur. Respir. J. 54, (2019).
95. Yamashita, M. et al. Distinct Profiles of CD163-Positive Macrophages in Idiopathic Interstitial Pneumonias. J Immunol Res 2018, 1436236 (2018).
96. Etzerodt, A. & Moestrup, S. K. CD163 and inflammation: biological, diagnostic, and therapeutic aspects. Antioxid. Redox Signal. 18, 2352–2363 (2013).
97. Chen, J.-M., Fortunato, M., Stevens, R. A. E. & Barrett, A. J. Activation of Progelatinase A by Mammalian Legumain, a Recently Discovered Cysteine Proteinase. 382, 777–784 (2001).
98. Kessenbrock, K., Plaks, V. & Werb, Z. Matrix metalloproteinases: regulators of the tumor microenvironment. Cell 141, 52–67 (2010).
99. AbdulHameed, M. D. M. et al. Systems level analysis and identification of pathways and networks associated with liver fibrosis. PLoS One 9, e112193 (2014).
100. Lunde, N. N. et al. Increased levels of legumain in plasma and plaques from patients with carotid atherosclerosis. Atherosclerosis 257, 216–223 (2017).
101. Remmerie, A. et al. Osteopontin Expression Identifies a Subset of Recruited Macrophages Distinct from Kupffer Cells in the Fatty Liver. Immunity 53, 641–657.e14 (2020).
102. Fastrès, A. et al. Identification of Pro-Fibrotic Macrophage Populations by Single-Cell Transcriptomic Analysis in West Highland White Terriers Affected With Canine Idiopathic Pulmonary Fibrosis. Front. Immunol. 11, 611749 (2020).
103. Berman, J. S. et al. Altered bleomycin-induced lung fibrosis in osteopontin-deficient mice. Am. J. Physiol. Lung Cell. Mol. Physiol. 286, L1311–8 (2004).
104. Rittling, S. R. & Denhardt, D. T. Osteopontin function in pathology: lessons from osteopontin-deficient mice. Exp. Nephrol. 7, 103–113 (1999).
105. Adler, M. et al. Principles of Cell Circuits for Tissue Repair and Fibrosis. iScience 23, 100841 (2020).
106. Soker, S., Takashima, S., Miao, H. Q., Neufeld, G. & Klagsbrun, M. Neuropilin-1 is expressed by endothelial and tumor cells as an isoform-specific receptor for vascular endothelial growth factor. Cell 92, 735–745 (1998).
107. Kofler, N. & Simons, M. The expanding role of neuropilin: regulation of transforming growth factor-β and platelet-derived growth factor signaling in the vasculature. Curr. Opin. Hematol. 23, 260–267 (2016).
108. Daly, J. L. et al. Neuropilin-1 is a host factor for SARS-CoV-2 infection. Science 370, 861–865 (2020).
109. Cantuti-Castelvetri, L. et al. Neuropilin-1 facilitates SARS-CoV-2 cell entry and infectivity. Science 370, 856–860 (2020).
110. Junttila, S., Smolander, J. & Elo, L. L. Benchmarking methods for detecting differential states between conditions from multi-subject single-cell RNA-seq data. bioRxiv 2022.02.16.480662 (2022) doi:10.1101/2022.02.16.480662.
111. Chua, R. L. et al. COVID-19 severity correlates with airway epithelium-immune cell interactions identified by single-cell analysis. Nat. Biotechnol. 38, 970–979 (2020).
112. Merad, M. & Martin, J. C. Pathological inflammation in patients with COVID-19: a key role for monocytes and macrophages. Nat. Rev. Immunol. 20, 355–362 (2020).

113. Blanco-Melo, D. et al. Imbalanced Host Response to SARS-CoV-2 Drives Development of COVID-19. Cell 181, 1036–1045.e9 (2020).

Eidesstattliche Versicherung

„Ich, Daniel Christian Wendisch versichere an Eides statt durch meine eigenhändige Unterschrift, dass ich die vorgelegte Dissertation mit dem Thema: „Macrophage and Monocyte Responses to SARS-CoV-2 / Analyse SARS-CoV-2-induzierter Makrophagen- und Monozytenphänotypen„ selbstständig und ohne nicht offengelegte Hilfe Dritter verfasst und keine anderen als die angegebenen Quellen und Hilfsmittel genutzt habe.
Alle Stellen, die wörtlich oder dem Sinne nach auf Publikationen oder Vorträgen anderer Autoren/innen beruhen, sind als solche in korrekter Zitierung kenntlich gemacht. Die Abschnitte zu Methodik (insbesondere praktische Arbeiten, Laborbestimmungen, statistische Aufarbeitung) und Resultaten (insbesondere Abbildungen, Graphiken und Tabellen) werden von mir verantwortet.

Ich versichere ferner, dass ich die in Zusammenarbeit mit anderen Personen generierten Daten, Datenauswertungen und Schlussfolgerungen korrekt gekennzeichnet und meinen eigenen Beitrag sowie die Beiträge anderer Personen korrekt kenntlich gemacht habe (siehe Anteilserklärung). Texte oder Textteile, die gemeinsam mit anderen erstellt oder verwendet wurden, habe ich korrekt kenntlich gemacht.

Meine Anteile an etwaigen Publikationen zu dieser Dissertation entsprechen denen, die in der untenstehenden gemeinsamen Erklärung mit dem/der Erstbetreuer/in, angegeben sind. Für sämtliche im Rahmen der Dissertation entstandenen Publikationen wurden die Richtlinien des ICMJE (International Committee of Medical Journal Editors; www.icmje.og) zur Autorenschaft eingehalten. Ich erkläre ferner, dass ich mich zur Einhaltung der Satzung der Charité – Universitätsmedizin Berlin zur Sicherung Guter Wissenschaftlicher Praxis verpflichte.

Weiterhin versichere ich, dass ich diese Dissertation weder in gleicher noch in ähnlicher Form bereits an einer anderen Fakultät eingereicht habe.

Die Bedeutung dieser eidesstattlichen Versicherung und die strafrechtlichen Folgen einer unwahren eidesstattlichen Versicherung (§§156, 161 des Strafgesetzbuches) sind mir bekannt und bewusst.“

Datum Unterschrift

Anteilserklärung an den erfolgten Publikationen

Daniel Christian Wendisch hatte folgenden Anteil an den folgenden Publikationen:

Publikation A

Daniel Wendisch*, Oliver Dietrich*, Tommaso Mari*, Saskia von Stillfried*, Ignacio L Ibarra, Mirja Mittermaier, Christin Mache, Robert Lorenz Chua, Rainer Knoll, Sara Timm, Sophia Brumhard, Tobias Krammer, Henrik Zauber, Anna Luisa Hiller, Anna Pascual-Reguant, Ronja Mothes, Roman David Bülow, Jessica Schulze, Alexander M Leipold, Sonja Djudjaj, Florian Erhard, Robert Geffers, Fabian Pott, Julia Kazmierski, Josefine Radke, Panagiotis Pergantis, Kevin Baßler, Claudia Conrad, Anna C Aschenbrenner, Birgit Sawitzki, Markus Landthaler, Emanuel Wyler, David Horst, Stefan Hippenstiel, Andreas Hocke, Frank L Heppner, Alexander Uhrig, Carmen Garcia, Felix Machleidt, Susanne Herold, Sefer Elezkurtaj, Charlotte Thibeault, Martin Witzenrath, Clément Cochain, Norbert Suttorp, Christian Drosten, Christine Goffinet, Florian Kurth, Joachim L Schultze, Helena Radbruch, Matthias Ochs, Roland Eils, Holger Müller-Redetzky, Anja E Hauser, Malte D Luecken, Fabian J Theis, Christian Conrad, Thorsten Wolff, Peter Boor, Matthias Selbach, Antoine-Emmanuel Saliba, Leif Erik Sander, Deutsche COVID-19 OMICS Initiative, **SARS-CoV-2 infection triggers profibrotic macrophage responses and lung fibrosis, Cell, 2021**

*=Erstautoren

Beitrag im Einzelnen:

Abbildung	Leistung	Beteiligte ErstautorInnen	weitere maßgeblich Beteiligte (außer Erst- und LetztautorenInnen)
1, S1	Durchführung MELC	**DW**	Anna Pascual-Reguant, Ronja Mothes, Anja E.Hauser, Helena Radbruch, Sonja Djudjaj, Peter Boor
	Bioinformatisch Analyse MELC	**DW, OD**	
	Immunohistochemie, Autopsien	**SvS**	
	Planung, Konzeption	**DW, OD, SvS**	
	Kuration Patientendaten	**DW, SvS**	
2, S2	Probenverarbeitung	**DW**	Sophia Brumhard, Mirja Mittermeier, Tobias Kramer, Holger Müller-Redezki
	Library preparation	**DW**	
	Bioinformatische Analyse	**DW, OD**	
	Planung, Konzeption	**DW, OD**	
	Kuration Patientendaten	**DW**	
3, S3	Probenverarbeitung	**DW**	Ignacia L. Ibarra, Malte D. Luecken, Sophia Brumhard, Mirja Mittermeier, Tobias Kramer, Holger Müller-Redezki
	Library preparation	**DW**	
	Bioinformatische Analyse	**DW, OD**	
	Planung, Konzeption	**DW, OD**	
4, S4	Bioinformatische Analyse snRNASeq, in Rücksprache	**DW, OD**	Lorenz Chua, Christian Conrad, Sonja Djudaj, Peter Boor, Anna Pascual-Reguant

	Planung, Konzeption	**DW, OD**	
	Immunfluoreszensmikroskopie	**SvS**	
	Analyse MELC	**DW**	
5, S5	Kuration Patientendaten	**DW, SvS**	
	Analyse Lungenmechanik	**DW**	
	Anlyse Computer Tomographie	**DW**	
	Histopathology	**SvS**	Mirja Mittermerier, Holger Müller-Redezki, Sonja Djudjaj, Peter Boor, Sara Timm, Matthias Ochs
6, S6	Durchführung Experimente	**DW**	
	Bioinformatische Analyse	**DW, OD**	Fabian Pott, Julia Kazmierski, Christine Goffinet
7, S7	Durchführung Experimente	**DW**	
	Probenaufarbeitung	**TM**	
	Bioinformatische Analyse	**TM**	
	Planung, Konzeption	**DW, OD, TM**	Christin Mache, Jessica Schulze, Henrik Zauber

Abkürzungen: DW: Daniel Wendisch; OD: Oliver Dietrich; SvS: Saskia von Stillfried; TM :Tommaso Mari

Die vorgelegte Arbeit erfolgte in enger und guter Kooperation der Erstautoren. Daniel Wendisch war führend beteiligt am experimentellen Teil der Arbeit sowie der Kuration der klinischen Daten von Kohorte 1, Oliver Dietrich war führend and der bioinformatischen Analyse beteiligt, Saskia v. Stillfried führte die Arbeiten zu Kohorte 2 an und Tommaso Mari war führend und maßgeblich an der Generierung und Analyse der proteomischen Daten beteiligt.

_____, den

Name (Druckbuchstaben):

Publikation B

Jonas Schulte-Schrepping*, Nico Reusch*, Daniela Paclik*, Kevin Baßler*, Stephan Schlickeiser*, Bowen Zhang*, Benjamin Krämer*, Tobias Krammer*, Sophia Brumhard*, Lorenzo Bonaguro*, Elena De Domenico*, **Daniel Wendisch***, Martin Grasshoff, Theodore S.Kapellos, Michael Beckstette, Tal Pecht, Adem Saglam, Oliver Dietrich, Henrik E.Mei, Axel R.Schulz, Claudia Conrad, Désirée Kunkel, Ehsan Vafadarnejad, Cheng-Jian Xu, Arik Horne, Miriam Herbert, Anna Drews, Charlotte Thibeault, Moritz Pfeiffer, Stefan Hippenstiel, Andreas Hocke, Holger Müller-Redetzky, Katrin-Moira Heim, Felix Machleidt, Alexander Uhrig, Laure Bosquillon de Jarcy, Linda Jürgens, Miriam Stegemann, Christoph R.Glösenkamp, Hans-Dieter Volk, Christine Goffinet, Markus Landthaler, Emanuel Wyler, Philipp Georg, Maria Schneider, Chantip Dang-Heine, Nick Neuwinger, Kai Kappert, Rudolf Tauber, Victor Corman, Jan Raabe, Kim Melanie Kaiser, Michael To Vinh, Gereon Rieke, Christian Meisel, Thomas Ulas, Matthias Becker, Robert Geffers, Martin Witzenrath, Christian Drosten, Norbert Suttorp, Christof von Kalle, Florian Kurth, Kristian

Händler, Joachim L.Schultze, Anna C. Aschenbrenner, Yang Li, Jacob Nattermann, Birgit Sawitzki, Antoine-Emmanuel Saliba, Leif Erik Sander, Deutsche COVID-19 OMICS Initiative (DeCOI), **Severe COVID-19 is marked by a dysregulated myeloid cell compartment, Cell,2020**

*=Erstautoren

Beitrag im Einzelnen:

Beschreibung des eigenen Anteils	**An den Abbildungen**
Beschaffung und Organisation der Patientendaten, Aufbau der Infrastruktur, Entwurf des Probenentnahme und -verarbeitungsprotokolls, Probenaufbearbeitung, Auswertung im Team	1C-D, 2A-C, 2E

_____

Unterschrift, Datum und Stempel des/der erstbetreuenden Hochschullehrers/in

_____

Unterschrift des Doktoranden/der Doktorandin

Auszug aus der Journal Summary List – Publikation A

Journal Data Filtered By: **Selected JCR Year: 2020** Selected Editions: SCIE,SSCI
Selected Categories: **"CELL BIOLOGY"** Selected Category Scheme: WoS
Gesamtanzahl: 195 Journale

Rank	Full Journal Title	Total Cites	Journal Impact Factor	Eigenfactor Score
1	NATURE REVIEWS MOLECULAR CELL BIOLOGY	58,477	94.444	0.075480
2	NATURE MEDICINE	114,401	53.440	0.184050
3	CELL	320,407	41.582	0.526960
4	CANCER CELL	50,839	31.743	0.081040
5	NATURE CELL BIOLOGY	52,554	28.824	0.070950
6	Cell Metabolism	52,192	27.287	0.091000
7	Journal of Extracellular Vesicles	8,485	25.841	0.011820
8	CELL RESEARCH	24,108	25.617	0.034400
9	Cell Stem Cell	32,147	24.633	0.062780
10	TRENDS IN CELL BIOLOGY	19,007	20.808	0.030120
11	Signal Transduction and Targeted Therapy	3,848	18.187	0.005730
12	MOLECULAR CELL	86,299	17.970	0.161840
13	Science Translational Medicine	45,509	17.956	0.103780
14	Autophagy	25,343	16.016	0.027970
15	CELL DEATH AND DIFFERENTIATION	27,701	15.828	0.028730
16	NATURE STRUCTURAL & MOLECULAR BIOLOGY	32,038	15.369	0.051210
17	Protein & Cell	5,352	14.870	0.009500
18	Annual Review of Cell and Developmental Biology	11,884	13.827	0.011100
19	DEVELOPMENTAL CELL	36,177	12.270	0.058350
20	TRENDS IN MOLECULAR MEDICINE	13,213	11.951	0.014720

Druckexemplar der Publikation A

Seiten 51-99

Wendisch, D. *et al*. SARS-CoV-2 infection triggers profibrotic macrophage responses and lung fibrosis. *Cell* **184**, 6243–6261.e27 (2021).

https://doi.org/10.1016/j.cell.2021.11.033

Auszug aus der Journal Summary List – Publikation B

Journal Data Filtered By: **Selected JCR Year: 2018** Selected Editions: SCIE,SSCI
Selected Categories: **"CELL BIOLOGY"** Selected Category Scheme: WoS
Gesamtanzahl: 193 Journale

Rank	Full Journal Title	Total Cites	Journal Impact Factor	Eigenfactor Score
1	NATURE REVIEWS MOLECULAR CELL BIOLOGY	45,869	43.351	0.091360
2	CELL	242,829	36.216	0.571850
3	NATURE MEDICINE	79,243	30.641	0.162840
4	CANCER CELL	36,056	23.916	0.091050
5	Cell Metabolism	34,829	22.415	0.099550
6	Cell Stem Cell	24,628	21.464	0.087030
7	CELL RESEARCH	15,131	17.848	0.038680
8	NATURE CELL BIOLOGY	40,615	17.728	0.082430
9	Science Translational Medicine	30,485	17.161	0.121980
10	TRENDS IN CELL BIOLOGY	14,380	16.588	0.034120
11	MOLECULAR CELL	62,812	14.548	0.170680
12	NATURE STRUCTURAL & MOLECULAR BIOLOGY	27,166	12.109	0.069440
13	EMBO JOURNAL	65,212	11.227	0.067930
14	Autophagy	16,161	11.059	0.032630
15	TRENDS IN MOLECULAR MEDICINE	9,946	11.028	0.018900
16	Journal of Extracellular Vesicles	3,675	11.000	0.012110
17	Annual Review of Cell and Developmental Biology	9,734	10.833	0.016750
18	AGEING RESEARCH REVIEWS	6,539	10.390	0.015890
19	CURRENT BIOLOGY	60,772	9.193	0.135820
20	DEVELOPMENTAL CELL	28,572	9.190	0.068550

Druckexemplar der Publikation B

Seiten 101-156

Schulte-Schrepping, J. et al. Severe COVID-19 Is Marked by a Dysregulated Myeloid Cell Compartment. Cell 182, 1419–1440.e23 (2020).

https://doi.org/10.1016/j.cell.2020.08.001

Mein Lebenslauf wird aus datenschutzrechtlichen Gründen in der elektronischen Version meiner Arbeit nicht veröffentlicht.

Publikationsliste

Daniel Wendisch

*** = Erstautoren**

2022

Aznaourova, Marina*; Schmerer, Nils*; Janga, Harshavardhan; Zhang, Zhenhua; Pauck, Kim; Bushe, Judith; Volkers, Sarah M; **Wendisch, Daniel**; Georg, Philipp; Ntini, Evgenia, … Schulte, L. N.; **Single-cell RNA sequencing uncovers the nuclear decoy lincRNA PIRAT as a regulator of systemic monocyte immunity during COVID-19, Proceedings of the National Academy of Sciences**,119,36,e2120680119,2022,National Academy of Sciences. Impact-Faktor (2020): 11.205

Pfäfflin, Frieder; **Wendisch, Daniel**; Scherer, Roland; Jürgens, Linda; Godzick-Njomgang, Gisèle; Tranter, Eva; Tober-Lau, Pinkus; Stegemann, Miriam Songa; Corman, Victor Max; Kurth, Florian; Schürmann, Drik. **Monkeypox in-patients with severe anal pain**, **Infection**,1-5,2022,Springer Berlin Heidelberg. Impact-Faktor (2021): 7.455

2021

Wendisch, D.*, Dietrich, O.*, Mari, T.*, von Stillfried, S.*, Ibarra, I. L., Mittermaier, M., Mache, C., Chua, R. L., Knoll, R., Timm, S., Brumhard, S., Krammer, T., Zauber, H., Hiller, A. L., Pascual-Reguant, A., Mothes, R., Bülow, R. D., Schulze, J., Leipold, A. M., … Sander, L. E. (2021). **SARS-CoV-2 infection triggers profibrotic macrophage responses and lung fibrosis. Cell**, 184(26), 6243–6261.e27. Impact-Faktor (2020): 41.582

2020

Kreye, J.*, Reincke, S. M.*, Kornau, H.-C., Sánchez-Sendin, E., Corman, V. M., Liu, H., Yuan, M., Wu, N. C., Zhu, X., Lee, C.-C. D., Trimpert, J., Höltje, M., Dietert, K., Stöffler, L., von Wardenburg, N., van Hoof, S., Homeyer, M. A., Hoffmann, J., Abdelgawad, A., …, Drosten, C. , **Wendisch, D**. ,Sander, L. E., Osterrieder, N., Wilson, I.,Prüss, H. (2020**). A Therapeutic Non-self-reactive SARS-CoV-2 Antibody Protects from Lung Pathology in a COVID-19 Hamster Model. Cell**, 183(4), 1058–1069.e19. Impact-Faktor (2018): 36,216

Braun, J.*, Loyal, L.*, Frentsch, M.*, **Wendisch, D.**, Georg, P., Kurth, F., Hippenstiel, S., Dingeldey, M., Kruse, B., Fauchere, F., Baysal, E., Mangold, M., Henze, L., Lauster, R., Mall, M. A., Beyer, K., Röhmel, J., Voigt, S., Schmitz, J., … Thiel, A. (2020**). SARS-CoV-2-reactive T cells in healthy donors and patients with COVID-19. Nature**, 587(7833), 270–274. Impact-Faktor (2018): 43.070

Schulte-Schrepping, J.*, Reusch, N.*, Paclik, D.*, Baßler, K.*, Schlickeiser, S.*, Zhang, B.*, Krämer, B.*, Krammer, T.*, Brumhard, S.*, Bonaguro, L.*, De Domenico, E.*, **Wendisch, D.***, Grasshoff, M., Kapellos, T. S., Beckstette, M., Pecht, T., Saglam, A., Dietrich, O., Mei, H. E., … Deutsche COVID-19 OMICS Initiative (DeCOI). (2020). **Severe COVID-19 Is Marked by a Dysregulated Myeloid Cell Compartment. Cell**, 182(6), 1419–1440.e23. Impact-Faktor (2018): 36,216

Chua, R. L.*, Lukassen, S.*, Trump, S.*, Hennig, B. P.*, **Wendisch, D.***, Pott, F., Debnath, O., Thürmann, L., Kurth, F., Völker, M. T., Kazmierski, J., Timmermann, B., Twardziok, S., Schneider, S., Machleidt, F., Müller-Redetzky, H., Maier, M., Krannich, A., Schmidt, S., … Eils, R. (2020). **COVID-19 severity correlates with airway epithelium-immune cell interactions identified by single-cell analysis. Nature Biotechnology**, 38(8), 970–979. Impact-Faktor (2018): 31.864

Messner, C.* B., Demichev, V.*, **Wendisch, D**., Michalick, L., White, M., Freiwald, A., Textoris-Taube, K., Vernardis, S. I., Egger, A.-S., Kreidl, M., Ludwig, D., Kilian, C., Agostini, F., Zelezniak, A., Thibeault, C., Pfeiffer, M., Hippenstiel, S., Hocke, A., von Kalle, C., … Ralser, M. (2020). **Ultra-High-Throughput Clinical Proteomics Reveals Classifiers of COVID-19 Infection. Cell Systems**, 11(1), 11–24.e4. Impact-Faktor (2018): 8.64

Patente

HUMAN RECOMBINANT MONOCLONAL ANTIBODY AGAINST SARS-COV-2 SPIKE GLYKOPROTEIN, International Publication Number WO 2021/239949 A1, 29 May 2021, Inventors: Kreye, J-.Prüss, H. Reincke, M., Kornau, H.-C., **Wendisch, D.,** Müller, M. A., Sander, L. E., Corman, V. M.

EICOV study group

Hillus, D., Schwarz, T., Tober-Lau, P., Vanshylla, K., Hastor, H., Thibeault, C., Jentzsch, S., Helbig, E. T., Lippert, L. J., Tscheak, P., Schmidt, M. L., Riege, J., Solarek, A., von Kalle, C., Dang-Heine, C., Gruell, H., Kopankiewicz, P., Suttorp, N., Drosten, C., … Sander, L. E. (2021). Safety, reactogenicity, and immunogenicity of homologous and heterologous prime-boost immunisation with ChAdOx1 nCoV-19 and BNT162b2: a prospective cohort study. The Lancet. Respiratory Medicine, 9(11), 1255–1265.Impact-Faktor (2019): 25.094

Pa-COVID-19 collaborative study group

Mühlemann, B., Thibeault, C., Hillus, D., Helbig, E. T., Lippert, L. J., Tober-Lau, P., Schwarz, T., Müller, M. A., Pa-COVID-19 collaborative study group, Witzenrath, M., Suttorp, N., Sander, L. E., Drosten, C., Jones, T. C., Corman, V. M., & Kurth, F. (2021). Impact of dexamethasone on SARS-CoV-2 concentra-

tion kinetics and antibody response in hospitalized COVID-19 patients: results from a prospective observational study. Clinical Microbiology and Infection: The Official Publication of the European Society of Clinical Microbiology and Infectious Diseases, 27(10), 1520.e7–e1520.e10. Impact-Faktor (2019): 8.067

Demichev, V., Tober-Lau, P., Lemke, O., Nazarenko, T., Thibeault, C., Whitwell, H., Röhl, A., Freiwald, A., Szyrwiel, L., Ludwig, D., Correia-Melo, C., Aulakh, S. K., Helbig, E. T., Stubbemann, P., Lippert, L. J., Grüning, N.-M., Blyuss, O., Vernardis, S., White, M., … Kurth, F. (2021). A time-resolved proteomic and prognostic map of COVID-19. Cell Systems, 12(8), 780–794.e7. Impact-Faktor (2019): 8.

Acknowledgements

I want to sincerely thank my supervisor Prof. Leif Erik Sander for the advice, support, discussions, drive, freedom to pursue own ideas and his mentorship during the years of my dissertation.
I am truly grateful for the kind support, collaborative spirit and the good times of, and together with so many colleagues and co-authors, especially during the intense phases of the Covid-19 pandemic.
Particularly, I want to thank Prof. Emmanuel Saliba and Prof. Annette Mankertz and their teams for teaching me many valuable methods and academic lessons.
I deeply want to appreciate the support of my great friends and family without whom this would not have been remotely possible or worthwhile.